

Epigraphical splitting for solving constrained convex formulations of inverse problems with proximal tools

G. Chierchia*, N. Pustelnik†, J.-C. Pesquet‡ and B. Pesquet-Popescu*

November 6, 2018

Abstract

We propose a proximal approach to deal with a class of convex variational problems involving nonlinear constraints. A large family of constraints, proven to be effective in the solution of inverse problems, can be expressed as the lower level set of a sum of convex functions evaluated over different, but possibly overlapping, blocks of the signal. For such constraints, the associated projection operator generally does not have a simple form. We circumvent this difficulty by splitting the lower level set into as many epigraphs as functions involved in the sum. A closed half-space constraint is also enforced, in order to limit the sum of the introduced epigraphical variables to the upper bound of the original lower level set. In this paper, we focus on a family of constraints involving linear transforms of distance functions to a convex set or $\ell_{1,p}$ norms with $p \in \{1, 2, +\infty\}$. In these cases, the projection onto the epigraph of the involved function has a closed form expression.

The proposed approach is validated in the context of image restoration with missing samples, by making use of constraints based on Non-Local Total Variation. Experiments show that our method leads to significant improvements in term of convergence speed over existing algorithms for solving similar constrained problems. A second application to a pulse shape design problem is provided in order to illustrate the flexibility of the proposed approach.

1 Introduction

As an offspring of the wide interest in frame representations and sparsity promoting techniques for data recovery, proximal methods have become popular for solving large-size non-smooth convex optimization problems [1,2,3]. The efficiency of these methods in the solution of inverse problems has been widely studied in the recent signal and image processing literature (see for instance [4,5,6,7,8,9] and references therein). Even if proximal algorithms and the associated convergence properties have been deeply investigated [10,11,12,13], some questions persist in their use for solving inverse problems. A first question is: how can we set the parameters serving to enforce the regularity

*Institut Mines-Télécom, Télécom ParisTech, CNRS LTCI, 75014 Paris, France

†ENS Lyon, Laboratoire de Physique, UMR CNRS 5672, F69007 Lyon, France

‡Université Paris-Est, LIGM, UMR CNRS 8049, 77454 Marne-la-Vallée, France

of the solution in an automatic way? Various strategies were proposed in order to address this question [14, 15, 16, 17, 18], but the computational cost of these methods is often high, especially when several regularization parameters have to be set. Alternatively, it has been recognized for a long time that incorporating constraints directly on the solutions [19, 20, 21, 22, 23, 24, 25], instead of considering regularized functions, may often facilitate the choice of the involved parameters. Indeed, in a constrained formulation, the constraint bounds are usually related to some physical properties of the target solution or some knowledge of the degradation process, e.g. the noise statistical properties. Note also that there exist some conceptual Lagrangian equivalences between regularized solutions to inverse problems and constrained ones, although some caution should be taken when the regularization functions are nonsmooth (see [26] where the case of a single regularization parameter is investigated).

Another question is related to the selection of the most appropriate algorithm within the class of proximal methods according to a given application. This also raises the question of the computation of the proximity operators associated with the different functions involved in the criterion. In this context, the objective of this paper is to propose an efficient splitting technique for solving some constrained convex optimization problems of the form:

Problem 1.1.

$$\underset{x \in \mathcal{H}}{\text{minimize}} \quad \sum_{r=1}^R g_r(T_r x) \quad \text{s. t.} \quad \begin{cases} H_1 x \in C_1, \\ \dots \\ H_S x \in C_S, \end{cases} \quad (1)$$

where \mathcal{H} is a real Hilbert space, and

- (i) for every $r \in \{1, \dots, R\}$, T_r is a bounded linear operator from \mathcal{H} to \mathbb{R}^{N_r} ,
- (ii) for every $r \in \{1, \dots, R\}$, $g_r: \mathbb{R}^{N_r} \mapsto]-\infty, +\infty]$ is a proper lower-semicontinuous convex function,
- (iii) for every $s \in \{1, \dots, S\}$, H_s is a bounded linear operator from \mathcal{H} to \mathbb{R}^{M_s} ,
- (iv) for every $s \in \{1, \dots, S\}$, C_s is a nonempty closed convex subset of \mathbb{R}^{M_s} .

More precisely, the present work aims at designing a method to address Problem 1.1 when some convex constraints are expressed as follows: for some $s \in \{1, \dots, S\}$,

$$(\forall x \in \mathcal{H}) \quad H_s x \in C_s \quad \Leftrightarrow \quad h_s(H_s x) \leq \eta_s, \quad (2)$$

where $\eta_s \in \mathbb{R}$ and h_s is a proper lower-semicontinuous convex function from \mathbb{R}^{M_s} to $]-\infty, +\infty]$. Indeed, the projection onto the convex set C_s defined in (2) often does not have a closed form expression. In the present work, we will show that:

- (i) when the function h_s in (2) corresponds to a *decomposable loss*, i.e. it can be expressed as the sum of functions evaluated over different blocks of the vector $H_s x$, the problem of computing the projection onto the associated convex set C_s can be addressed by resorting to a splitting approach that decomposes the set C_s into a collection of epigraphs and a half-space;

- (ii) the projection operator associated with an epigraph (namely the *epigraphical projection*) has a closed form for some functions of practical interest, such as the absolute value raised to a power $q \in [1, +\infty[$, the distance to a convex set and the ℓ_p -norm with $p \in \{2, +\infty\}$;
- (iii) in the context of image restoration, regularity constraints based on Total Variation [27] and Non-Local Total Variation [28] can be efficiently handled by the proposed epigraphical splitting, which significantly speeds up the convergence (in terms of execution time) with respect to standard iterative solutions [29, 30].

The paper is organized as follows. In Section 2, we review the algorithms which are applicable for solving large-size convex optimization problems, so motivating the choice of proximal methods, and we review the variable-splitting techniques commonly used with these methods. In order to deal with a constraint expressed under the form (2), we propose in section 3 a novel splitting approach involving an epigraphical projection. In addition, closed form expressions for specific epigraphical projections are given. Experiments in two different contexts are presented in Section 4. The first ones concern an image reconstruction problem, while the second ones are related to pulse shape design for digital communications. Finally, some conclusions are drawn in Section 5.

Notation: Let \mathcal{H} be a real Hilbert space endowed with the norm $\|\cdot\|$ and the scalar product $\langle \cdot | \cdot \rangle$. $\Gamma_0(\mathcal{H})$ denotes the set of proper lower-semicontinuous convex functions from \mathcal{H} to $] -\infty, +\infty]$. The epigraph of $\varphi \in \Gamma_0(\mathcal{H})$ is the nonempty closed convex subset of $\mathcal{H} \times \mathbb{R}$ defined as $\text{epi } \varphi = \{(y, \zeta) \in \mathcal{H} \times \mathbb{R} \mid \varphi(y) \leq \zeta\}$ and the lower level set of φ at height $\zeta \in \mathbb{R}$ is the nonempty closed convex subset of \mathcal{H} defined as $\text{lev}_{\leq \zeta} \varphi = \{y \in \mathcal{H} \mid \varphi(y) \leq \zeta\}$. A subgradient of φ at $y \in \mathcal{H}$ is an element of its subdifferential defined as $\partial\varphi(y) = \{t \in \mathcal{H} \mid (\forall u \in \mathcal{H}) \varphi(u) \geq \varphi(y) + \langle t | u - y \rangle\}$. When φ is Gâteaux-differentiable at y , $\partial\varphi(y) = \{\nabla\varphi(y)\}$ where $\nabla\varphi(y)$ is the gradient of φ at y . Let C be a nonempty closed convex subset C of \mathcal{H} . The relative interior of C is denoted by $\text{ri } C$. For every $y \in \mathcal{H}$, the indicator function $\iota_C \in \Gamma_0(\mathcal{H})$ of C is given by

$$\iota_C(y) = \begin{cases} 0, & \text{if } y \in C, \\ +\infty, & \text{otherwise,} \end{cases} \quad (3)$$

the projection onto C reads $P_C(y) = \text{argmin}_{u \in C} \|u - y\|$, and the distance to C is given by $d_C(y) = \|y - P_C(y)\|$.

2 Proximal tools

2.1 From gradient descent to proximal algorithms

The first methods for finding a solution to an inverse problem were restricted to the use of a differentiable cost function [31], i.e. Problem 1.1 where $S = 0$ and, for every $r \in \{1, \dots, R\}$, g_r denotes a differentiable function. In this context, gradient-based algorithms appear to be the most efficient solutions when an iterative procedure is required (see [32] and references therein). However, in order to model additional properties, sparsity promoting penalizations ($R \geq 1$) or hard

constraints ($S \geq 1$) may be introduced and the differentiability property is not satisfied anymore. One way to circumvent this difficulty is to resort to smart approximations in order to smooth the involved non-differentiable functions [33, 34, 35, 36]. If one wants to address the original nonsmooth problem without approximation errors, one may apply some specific algorithms [37], the convergence of which is guaranteed under restrictive assumptions. Interior point methods [38] can also be employed for small to medium size optimization problems.

On the other hand, in order to solve convex feasibility problems, i.e. to find a vector belonging to the intersection of convex sets (Problem 1.1 with $R = 0$), iterative projection methods were developed. The projection onto convex sets algorithm (POCS) is one of the most popular approach to solve data recovery problems [19, 39, 40, 41]. A drawback of POCS is that it is not well-suited for parallel implementations. The Parallel Projection Method (PPM) and Method of Parallel Projections (MOPP) are variants of POCS making use of parallel projections. Moreover, these algorithms were designed to efficiently solve inconsistent feasibility problems (when the intersection of the convex set is empty). Thorough comparisons between projection methods have been performed in [42, 43].

Computing the projection P_C onto a nonempty closed convex subset C of a real Hilbert space \mathcal{H} requires to solve a constrained quadratic minimization problem. However, it turns out that a closed form expression of the solution to this problem is available in a limited number of instances. Some well-known examples are the projections onto hyperplanes, closed half-spaces and ℓ_2 -norm balls [36, 44]. When an expression of the direct projection is not available, the convex set C can be approximated by a half-space, which leads to the concept of subgradient projection. An efficient block iterative surrogate splitting method was proposed in [45] in order to solve Problem 1.1 when $S \geq 1$ and, for every $r \in \{1, \dots, R\}$, $g_r = \|\cdot - z_r\|^2$ where $z_r \in \mathbb{R}^{N_r}$. A main limitation of this method is that the global objective function must be strictly convex. For recent works about subgradient projection methods, the readers may refer to [46, 47, 48].

A way to overcome this difficulty consists of considering proximal approaches. The key tool in these methods is the proximity operator [49] of a function $\varphi \in \Gamma_0(\mathcal{H})$, defined as

$$(\forall y \in \mathcal{H}) \quad \text{prox}_\varphi(y) = \underset{u \in \mathcal{H}}{\operatorname{argmin}} \frac{1}{2} \|u - y\|^2 + \varphi(u). \quad (4)$$

The proximity operator can be interpreted as a sort of subgradient step for the function φ , as $p = \text{prox}_\varphi(y)$ is uniquely defined through the inclusion

$$y - p \in \partial\varphi(p). \quad (5)$$

Proximity operators enjoy many interesting properties [11]. In particular, they generalize the notion of projection onto a closed convex set C , in the sense that $\text{prox}_{\iota_C} = P_C$. Hence, proximal methods provide a unifying framework that allows one to address non-smooth penalizations ($R \geq 1$) and hard constraints ($S \geq 1$).

The class of proximal methods includes primal algorithms [2, 11, 12, 50, 51, 52, 53, 54, 55] and primal-dual algorithms [56, 57, 58, 59, 60, 61, 62, 63]. Primal algorithms generally require to inverse some linear operators (e.g. $\sum_{r=1}^R T_r^* T_r + \sum_{s=1}^S H_s^* H_s$), while primal-dual ones only require to compute $(T_r)_{1 \leq r \leq R}$, $(H_s)_{1 \leq s \leq S}$ and their adjoints. Consequently, primal-dual methods are often

easier to implement than primal ones, but their convergence may be slower [64, 65]. Note also that some of these methods are closely related to augmented Lagrangian approaches [66, 67].

2.2 Variable-splitting techniques

With the development of proximal methods for solving convex optimization problems, many techniques have been developed to cope with the intrinsic limitations of these methods. In particular, the computation of the proximity operator becomes intractable in general when considering the sum of several functions or a function composed with a linear operator. In this context, variable-splitting constitutes a very effective way to design easily implementable algorithms. One of the most popular examples is given by the approaches inspired by the Alternating Direction Method of Multipliers (ADMM), which deal with optimization problems of the form

$$\underset{x \in \mathcal{H}}{\text{minimize}} \quad g_1(T_1 x) + g_2(x). \quad (6)$$

By introducing an auxiliary variable $v \in \mathbb{R}^{N_1}$, the problem is reformulated as

$$\underset{(x,v) \in \mathcal{H} \times \mathbb{R}^{N_1}}{\text{minimize}} \quad g_1(v) + g_2(x) \quad \text{s. t.} \quad T_1 x = v. \quad (7)$$

This kind of splitting technique has been often used in image restoration [66, 68] and more recently for distributed optimization problems [69]. A similar form of splitting has been considered in [7, 70], where the constraint $T_1 x = v$ is handled by computing the projection onto the nullspace of the linear operator $[T_1 \quad -\text{Id}]$, which has a closed-form expression for some specific choices of T_1 , such as circulant matrices involved in image restoration.

The solution that we will propose in this work also introduces auxiliary variables. However, our objective is not to deal with linear transformations of the data but with a projection which does not have a closed-form expression. Consequently, the proposed solution departs from the usual splitting methods, in the sense that our approach leads to a collection of epigraphs and a half-space constraint sets, while the usual splitting techniques yield linear constraints.

3 Proposed method

We now turn our attention to convex sets for which the associated projection does not have a closed form and we show that, under some appropriate assumptions, it is possible to circumvent this difficulty. In Problem 1.1, assume that C_1 denotes such a constraint and that it can be modelled as: for every $y \in \mathbb{R}^{M_1}$,

$$y \in C_1 \quad \Leftrightarrow \quad h_1(y) = \sum_{\ell=1}^{L_1} h_1^{(\ell)}(y^{(\ell)}) \leq \eta_1 \quad (8)$$

where $\eta_1 \in \mathbb{R}$. Hereabove, the generic vector y has been decomposed into blocks of coordinates as follows

$$y = [\underbrace{(y^{(1)})^\top}_{\text{size } M_1^{(1)}}, \dots, \underbrace{(y^{(L_1)})^\top}_{\text{size } M_1^{(L_1)}}]^\top \quad (9)$$

and, for every $\ell \in \{1, \dots, L_1\}$, $y^{(\ell)} \in \mathbb{R}^{M_1^{(\ell)}}$ and $h_1^{(\ell)}$ is a function in $\Gamma_0(\mathbb{R}^{M_1^{(\ell)}})$ such that $\text{ri}(\text{dom } h_1^{(\ell)}) \neq \emptyset$.

3.1 Epigraphical splitting

The idea underlying our approach consists of introducing an auxiliary vector $\zeta_1 = (\zeta_1^{(\ell)})_{1 \leq \ell \leq L_1} \in \mathbb{R}^{L_1}$, so that Constraint (8) can be equivalently rewritten as^{* 0}

$$\begin{cases} \sum_{\ell=1}^{L_1} \zeta_1^{(\ell)} \leq \eta_1, \\ (\forall \ell \in \{1, \dots, L_1\}) \quad h_1^{(\ell)}(y^{(\ell)}) \leq \zeta_1^{(\ell)}. \end{cases} \quad (10)$$

$$\quad (11)$$

Let us now introduce the closed half-space of \mathbb{R}^{L_1} defined as

$$V_1 = \{\zeta \in \mathbb{R}^{L_1} \mid \mathbf{1}_{L_1}^\top \zeta \leq \eta_1\}, \quad (12)$$

with $\mathbf{1}_{L_1} = (1, \dots, 1)^\top \in \mathbb{R}^{L_1}$, and the closed convex set

$$E_1 = \{(y, \zeta) \in \mathbb{R}^{M_1} \times \mathbb{R}^{L_1} \mid (\forall \ell \in \{1, \dots, L_1\}) (y^{(\ell)}, \zeta^{(\ell)}) \in \text{epi } h_1^{(\ell)}\}. \quad (13)$$

Then, Constraint (10) means that $\zeta_1 \in V_1$, while Constraint (11) is equivalent to $(y, \zeta_1) \in E_1$. In other words, the constraint C_1 can be split into the two constraints V_1 and E_1 , provided that an additional vector $\zeta_1 \in \mathbb{R}^{L_1}$ is introduced in Problem 1.1. The resulting criterion takes the form:

Problem 3.1.

$$\begin{aligned} & \underset{(x, \zeta_1) \in \mathcal{H} \times V_1}{\text{minimize}} \quad \sum_{r=1}^R g_r(T_r x) \quad \text{s. t.} \quad \begin{cases} (H_1 x, \zeta_1) \in E_1 \\ H_2 x \in C_2 \\ \vdots \\ H_S x \in C_S. \end{cases} \end{aligned} \quad (14)$$

Note that the additional constraints can be easily handled by proximal algorithms as far as the projections onto the associated constraint sets can be computed. In the present case, the projection onto V_1 is well-known [36], whereas the projection onto E_1 is given by

$$(\forall (y, \zeta) \in \mathbb{R}^{M_1} \times \mathbb{R}^{L_1}) \quad P_{E_1}(y, \zeta) = (p, \theta) \quad (15)$$

where $\theta = (\theta^{(\ell)})_{1 \leq \ell \leq L_1}$, vector $p \in \mathbb{R}^{M_1}$ is blockwise decomposed as $p = [(\mathbf{p}^{(1)})^\top, \dots, (\mathbf{p}^{(L_1)})^\top]^\top$ like in (9), and

$$(\forall \ell \in \{1, \dots, L_1\}) \quad (\mathbf{p}^{(\ell)}, \theta^{(\ell)}) = P_{\text{epi } h_1^{(\ell)}}(y^{(\ell)}, \zeta^{(\ell)}). \quad (16)$$

Hence, the problem reduces to the lower-dimensional problem of the determination of the projection onto the convex subset $\text{epi } h_1^{(\ell)}$ of $\mathbb{R}^{M_1^{(\ell)}} \times \mathbb{R}$ for each $\ell \in \{1, \dots, L_1\}$. An example of an algorithm that converges to a solution to Problem 3.1 will be provided in Section 4.

^{0*}Note that the inequality in (10) can be also replaced by an equality, even though it makes little difference in our approach.

3.2 Proximity operators: new closed forms

The key point in the proposed splitting is the introduction of some epigraphs in the minimization process. In the following, we provide some results concerning the projection onto the epigraph of a convex function.

Proposition 3.2. *Let \mathcal{H} be a real Hilbert space and let $\mathcal{H} \times \mathbb{R}$ be equipped with the standard product space norm. Let φ be a function in $\Gamma_0(\mathcal{H})$ such that $\text{dom } \varphi$ is open. The projector $P_{\text{epi } \varphi}$ onto the epigraph of φ is given by:*

$$(\forall (y, \zeta) \in \mathcal{H} \times \mathbb{R}) \quad P_{\text{epi } \varphi}(y, \zeta) = (p, \theta) \quad (17)$$

where

$$\begin{cases} p &= \text{prox}_{\frac{1}{2}(\max\{\varphi - \zeta, 0\})^2}(y), \\ \theta &= \max\{\varphi(p), \zeta\}. \end{cases} \quad (18)$$

Proof. For every $(y, \zeta) \in \mathcal{H} \times \mathbb{R}$, let $(p, \theta) = P_{\text{epi } \varphi}(y, \zeta)$. If $\varphi(y) \leq \zeta$, then $p = y$ and $\theta = \zeta = \max\{\varphi(p), \zeta\}$. In addition,

$$\begin{aligned} (\forall u \in \mathcal{H}) \quad 0 &= \frac{1}{2}\|p - y\|^2 + \frac{1}{2}(\max\{\varphi(p) - \zeta, 0\})^2 \\ &\leq \frac{1}{2}\|u - y\|^2 + \frac{1}{2}(\max\{\varphi(u) - \zeta, 0\})^2, \end{aligned} \quad (19)$$

which shows that (18) holds. Let us now consider the case when $\varphi(y) > \zeta$. From the definition of the projection, we get

$$(p, \theta) = \underset{(u, \xi) \in \text{epi } \varphi}{\text{argmin}} \quad \|u - y\|^2 + (\xi - \zeta)^2. \quad (20)$$

From the Karush-Kuhn-Tucker theorem [71, Theorem 5.2],^{*} there exists $\alpha \in [0, +\infty[$ such that

$$(p, \theta) = \underset{(u, \xi) \in \mathcal{H} \times \mathbb{R}}{\text{argmin}} \quad \frac{1}{2}\|u - y\|^2 + \frac{1}{2}(\xi - \zeta)^2 + \alpha(\varphi(u) - \xi) \quad (21)$$

where the Lagrange multiplier α is such that $\alpha(\varphi(p) - \theta) = 0$. Since the value $\alpha = 0$ is not allowable (since it would lead to $p = y$ and $\theta = \zeta$), it can be deduced from the above equality that $\varphi(p) = \theta$. In addition, differentiating the Lagrange functional in (21) w.r.t. ξ yields

$$\varphi(p) = \theta = \zeta + \alpha \geq \zeta. \quad (22)$$

Hence, (p, θ) given by (20) is such that

$$p = \underset{\substack{u \in \mathcal{H} \\ \varphi(u) \geq \zeta}}{\text{argmin}} \quad \|u - y\|^2 + (\varphi(u) - \zeta)^2 \quad (23)$$

$$\theta = \varphi(p) = \max\{\varphi(p), \zeta\}. \quad (24)$$

^{*}By considering $u_0 \in \text{dom } \varphi$ and $\xi_0 > \varphi(u_0)$, the required qualification condition is obviously satisfied.

Furthermore, as $\varphi(y) > \zeta$, we have

$$\inf_{\substack{u \in \mathcal{H} \\ \varphi(u) \leq \zeta}} \|u - y\|^2 = \|P_{\text{lev}_{\leq \zeta} \varphi}(y) - y\|^2 = \inf_{\substack{u \in \mathcal{H} \\ \varphi(u) = \zeta}} \|u - y\|^2 \quad (25)$$

where we have used the fact that $P_{\text{lev}_{\leq \zeta} \varphi}(y)$ belongs to the boundary of $\text{lev}_{\leq \zeta} \varphi$ which is equal to $\{u \in \mathcal{H} \mid \varphi(u) = \zeta\}$ since φ is lower-semicontinuous and $\text{dom } \varphi$ is open [44, Corollary 8.38]. We have then

$$\begin{aligned} \inf_{\substack{u \in \mathcal{H} \\ \varphi(u) \leq \zeta}} \|u - y\|^2 &= \inf_{\substack{u \in \mathcal{H} \\ \varphi(u) = \zeta}} \|u - y\|^2 \\ &\geq \inf_{\substack{u \in \mathcal{H} \\ \varphi(u) \geq \zeta}} \|u - y\|^2 + (\varphi(u) - \zeta)^2. \end{aligned} \quad (26)$$

Altogether, (23) and (26) lead to

$$p = \operatorname{argmin}_{u \in \mathcal{H}} \frac{1}{2} \|u - y\|^2 + \frac{1}{2} (\max\{\varphi(u) - \zeta, 0\})^2 \quad (27)$$

which is equivalent to (18) since $\frac{1}{2} (\max\{\varphi - \zeta, 0\})^2 \in \Gamma_0(\mathcal{H})$. \square

Note that alternative characterizations of the epigraphical projection can be found in [44, Propositions 9.17, 28.28].

From the previous proposition, we see that the proximity operator in (18) plays a prominent role in the calculation of the projection onto $\text{epi } \varphi$. We now provide an example of function φ for which this proximity operator admits a simple form.

Proposition 3.3. *Let $\beta \in [1, +\infty[$, $\tau \in]0, +\infty[$. Assume that*

$$(\forall y \in \mathbb{R}) \quad \varphi(y) = \tau |y|^\beta. \quad (28)$$

If $\zeta \in]-\infty, 0]$, then for every $y \in \mathbb{R}$

$$\operatorname{prox}_{\frac{1}{2}(\max\{\tau|\cdot|^\beta - \zeta, 0\})^2}(y) = \begin{cases} \frac{\operatorname{sign}(y)}{1 + \tau^2} \max\{|y| + \tau\zeta, 0\}, & \text{if } \beta = 1, \\ \operatorname{sign}(y)\chi_0, & \text{if } \beta > 1, \end{cases} \quad (29)$$

where χ_0 is the unique solution on $[0, +\infty[$ of the equation

$$\beta\tau^2\chi^{2\beta-1} - \beta\tau\zeta\chi^{\beta-1} + \chi = |y|. \quad (30)$$

If $\zeta \in]0, +\infty[$, then, for every $y \in \mathbb{R}$,

$$\operatorname{prox}_{\frac{1}{2}(\max\{\tau|\cdot|^\beta - \zeta, 0\})^2}(y) = \begin{cases} y, & \text{if } \tau|y|^\beta \leq \zeta, \\ \operatorname{sign}(y)\chi_\zeta, & \text{otherwise,} \end{cases} \quad (31)$$

where χ_ζ is the unique solution on $[(\frac{\zeta}{\tau})^{1/\beta}, +\infty[$ of (30).

Proof. Since $(\max\{\varphi - \zeta, 0\})^2$ is an even function, $\text{prox}_{\frac{1}{2}(\max\{\varphi - \zeta, 0\})^2}$ is an odd function [11, Remark 4.1(ii)]. In the following, we thus focus on the case when $y \in]0, +\infty[$. If $\zeta \in]-\infty, 0]$, then $(\max\{\varphi - \zeta, 0\})^2 = (\varphi - \zeta)^2$. When $\beta = 1$, $\frac{1}{2}(\max\{\varphi - \zeta, 0\})^2 = (\tau^2/2)(\cdot)^2 - \tau\zeta|\cdot| + \zeta^2/2$ and, from [11, Example 4.6], it can be deduced that

$$\text{prox}_{\frac{1}{2}(\max\{\varphi - \zeta, 0\})^2}(y) = \frac{1}{1 + \tau^2} \max\{y + \tau\zeta, 0\}. \quad (32)$$

When $\beta > 1$, $(\varphi - \zeta)^2$ is differentiable and, according to (5), $p = \text{prox}_{\frac{1}{2}(\max\{\varphi - \zeta, 0\})^2}(y)$ is uniquely defined as

$$p - y + \beta\tau p^{\beta-1}(\tau p^\beta - \zeta) = 0 \quad (33)$$

where, according to [72, Corollary 2.5], $p \geq 0$. This allows us to deduce that $p = \chi_0$.

Let us now focus on the case when $\zeta \in]0, +\infty[$. If $y \in]0, (\zeta/\tau)^{1/\beta}[$, it can be deduced from [72, Corollary 2.5], that $p = \text{prox}_{\frac{1}{2}(\max\{\varphi - \zeta, 0\})^2}(y) \in [0, (\zeta/\tau)^{1/\beta}[$. Since $(\forall v \in [0, (\zeta/\tau)^{1/\beta}[) \max\{\varphi(v) - \zeta, 0\} = 0$, (5) yields $p = y$. On the other hand if $y > (\zeta/\tau)^{1/\beta}$, as the proximity operator of a function from \mathbb{R} to \mathbb{R} is continuous and increasing [72, Proposition 2.4], $p = \text{prox}_{\frac{1}{2}(\max\{\varphi - \zeta, 0\})^2}(y) \geq \text{prox}_{\frac{1}{2}(\max\{\varphi - \zeta, 0\})^2}((\zeta/\tau)^{1/\beta}) = (\zeta/\tau)^{1/\beta}$. Since $(\max\{\varphi - \zeta, 0\})^2$ is differentiable in this case, and $(\forall v \geq (\zeta/\tau)^{1/\beta}) (\max\{\varphi(v) - \zeta, 0\})^2 = (\tau v^\beta - \zeta)^2$, (5) allows us to deduce that p is the unique value in $[(\zeta/\tau)^{1/\beta}, +\infty[$ satisfying (33). It can be concluded that, when $\zeta \in]0, +\infty[$, (31) holds. \square

Note that, when β is a rational number, (30) is equivalent to a polynomial equation for which either closed form solutions are known or standard numerical solutions exist.

3.3 Examples of epigraphical projections

The previous propositions allow us to establish the following results concerning the epigraphical projection in (16):^{* 0}

- Distance functions of the form

$$(\forall \mathbf{y}^{(\ell)} \in \mathbb{R}^{M^{(\ell)}}) \quad h^{(\ell)}(\mathbf{y}^{(\ell)}) = \tau^{(\ell)} d_{C^{(\ell)}}^{\beta^{(\ell)}}(\mathbf{y}^{(\ell)}) \quad (34)$$

where $\ell \in \{1, \dots, L\}$, $\tau^{(\ell)} \in]0, +\infty[$, $\beta^{(\ell)} \in [1, +\infty]$, and $C^{(\ell)}$ is a nonempty closed convex subset of $\mathbb{R}^{M^{(\ell)}}$.

Proposition 3.4. *Assume that $h^{(\ell)}$ is given by (34). Then, for every $(\mathbf{y}^{(\ell)}, \zeta^{(\ell)}) \in \mathbb{R}^{M^{(\ell)}} \times \mathbb{R}$, $P_{\text{epi } h^{(\ell)}}(\mathbf{y}^{(\ell)}, \zeta^{(\ell)}) = (\mathbf{p}^{(\ell)}, \theta^{(\ell)})$ where*

$$\mathbf{p}^{(\ell)} = \begin{cases} \mathbf{y}^{(\ell)}, & \text{if } \mathbf{y}^{(\ell)} \in C^{(\ell)}, \\ \alpha^{(\ell)} \mathbf{y}^{(\ell)} + (1 - \alpha^{(\ell)}) P_{C^{(\ell)}}(\mathbf{y}^{(\ell)}), & \text{otherwise,} \end{cases} \quad (35)$$

^{0*}We drop the subscript from h_1 , M_1 and L_1 in order to relieve the notations.

and $\theta^{(\ell)} = \max\{\tau^{(\ell)} d_{C^{(\ell)}}^{\beta^{(\ell)}}(\mathbf{p}^{(\ell)}), \zeta^{(\ell)}\}$, where

$$\alpha^{(\ell)} = \frac{\text{prox}_{\frac{1}{2}(\max\{\tau^{(\ell)}|\cdot|^{\beta^{(\ell)}} - \zeta^{(\ell)}, 0\})^2}(d_{C^{(\ell)}}(\mathbf{y}^{(\ell)}))}{d_{C^{(\ell)}}(\mathbf{y}^{(\ell)})} \quad (36)$$

and the expression of $\text{prox}_{\frac{1}{2}(\max\{\tau^{(\ell)}|\cdot|^{\beta^{(\ell)}} - \zeta^{(\ell)}, 0\})^2}$ is provided by Proposition 3.3.

Proof.

Let us notice that $\frac{1}{2}(\max\{\tau^{(\ell)} d_{C^{(\ell)}}^{\beta^{(\ell)}} - \zeta^{(\ell)}, 0\})^2 = \psi^{(\ell)} \circ d_{C^{(\ell)}}$ where $\psi^{(\ell)} = \frac{1}{2}(\max\{\tau^{(\ell)}|\cdot|^{\beta^{(\ell)}} - \zeta^{(\ell)}, 0\})^2$. According to [13, Proposition 2.7], for every $\mathbf{y}^{(\ell)} \in \mathbb{R}^{M^{(\ell)}}$,

$$\text{prox}_{\psi^{(\ell)} \circ d_{C^{(\ell)}}}(\mathbf{y}^{(\ell)}) = \begin{cases} \mathbf{y}^{(\ell)}, & \text{if } \mathbf{y}^{(\ell)} \in C^{(\ell)}, \\ P_{C^{(\ell)}}(\mathbf{y}^{(\ell)}), & \text{if } d_{C^{(\ell)}}(\mathbf{y}^{(\ell)}) \leq \max \partial \psi^{(\ell)}(0), \\ \alpha^{(\ell)} \mathbf{y}^{(\ell)} + (1 - \alpha^{(\ell)}) P_{C^{(\ell)}}(\mathbf{y}^{(\ell)}), & \text{if } d_{C^{(\ell)}}(\mathbf{y}^{(\ell)}) > \max \partial \psi^{(\ell)}(0) \end{cases} \quad (37)$$

where $\alpha^{(\ell)} = \frac{\text{prox}_{\psi^{(\ell)}}(d_{C^{(\ell)}}(\mathbf{y}^{(\ell)}))}{d_{C^{(\ell)}}(\mathbf{y}^{(\ell)})}$. In addition, we have

$$\partial \psi^{(\ell)}(0) = \begin{cases} [\tau^{(\ell)} \zeta^{(\ell)}, -\tau^{(\ell)} \zeta^{(\ell)}], & \text{if } \zeta^{(\ell)} < 0 \text{ and } \beta^{(\ell)} = 1, \\ \{0\}, & \text{otherwise,} \end{cases} \quad (38)$$

and, according to Proposition 3.3, when $\zeta^{(\ell)} < 0$, $\beta^{(\ell)} = 1$ and $d_{C^{(\ell)}}(\mathbf{y}^{(\ell)}) \leq -\tau^{(\ell)} \zeta^{(\ell)}$, $\text{prox}_{\psi^{(\ell)}}(d_{C^{(\ell)}}(\mathbf{y}^{(\ell)})) = 0$. These show that (37) reduces to (35). \square

- Euclidean norms, as particular case of distance functions in (34) when $\beta^{(\ell)} \equiv 1$ and $C^{(\ell)} = \{0\}$:

$$(\forall \mathbf{y}^{(\ell)} \in \mathbb{R}^{M^{(\ell)}}) \quad h^{(\ell)}(\mathbf{y}^{(\ell)}) = \tau^{(\ell)} \|\mathbf{y}^{(\ell)}\| \quad (39)$$

where $\ell \in \{1, \dots, L\}$ and $\tau^{(\ell)} \in]0, +\infty[$. The resulting epigraphical projection is given below.

Corollary 3.5. Assume that $h^{(\ell)}$ is given by (39).

Then, for every $(\mathbf{y}^{(\ell)}, \zeta^{(\ell)}) \in \mathbb{R}^{M^{(\ell)}} \times \mathbb{R}$,

$$P_{\text{epi } h^{(\ell)}}(\mathbf{y}^{(\ell)}, \zeta^{(\ell)}) = \begin{cases} (0, 0), & \text{if } \|\mathbf{y}^{(\ell)}\| < -\tau^{(\ell)} \zeta^{(\ell)}, \\ (\mathbf{y}^{(\ell)}, \zeta^{(\ell)}), & \text{if } \|\mathbf{y}^{(\ell)}\| < \frac{\zeta^{(\ell)}}{\tau^{(\ell)}}, \\ \alpha^{(\ell)} (\mathbf{y}^{(\ell)}, \tau^{(\ell)} \|\mathbf{y}^{(\ell)}\|), & \text{otherwise,} \end{cases} \quad (40)$$

where $\alpha^{(\ell)} = \frac{1}{1 + (\tau^{(\ell)})^2} \left(1 + \frac{\tau^{(\ell)} \zeta^{(\ell)}}{\|\mathbf{y}^{(\ell)}\|}\right)$.

The epigraph of the Euclidean norm is the so-called Lorentz convex symmetric cone [73, 74] and the above result is actually known in the literature [75]. As it will be shown in Section 4, this expression of the epigraphical projection is useful to deal with multivariate sparsity constraints [76] or total variation bounds [27, 77], since such constraints typically involve a sum of functions like (39) composed with linear operators corresponding to analysis transforms or gradient operators.

- Infinity norms defined as: for every $\ell \in \{1, \dots, L\}$ and $\mathbf{y}^{(\ell)} = (\mathbf{y}^{(\ell, m)})_{1 \leq m \leq M^{(\ell)}} \in \mathbb{R}^{M^{(\ell)}}$,

$$h^{(\ell)}(\mathbf{y}^{(\ell)}) = \max \left\{ \frac{|\mathbf{y}^{(\ell, m)}|}{\tau^{(\ell, m)}} \mid 1 \leq m \leq M^{(\ell)} \right\}. \quad (41)$$

where $(\tau^{(\ell, m)})_{1 \leq m \leq M^{(\ell)}} \in]0, +\infty[^{M^{(\ell)}}$.

Proposition 3.6. *Assume that $h^{(\ell)}$ is given by (41) where the values $(\nu^{(\ell, m)} = |\mathbf{y}^{(\ell, m)}|/\tau^{(\ell, m)})_{1 \leq m \leq M^{(\ell)}}$ are in ascending order, and set $\nu^{(\ell, 0)} = -\infty$ and $\nu^{(\ell, M^{(\ell)}+1)} = +\infty$. Then, for every $\zeta^{(\ell)} \in \mathbb{R}$, $(\mathbf{p}^{(\ell)}, \theta^{(\ell)}) = P_{\text{epi } h^{(\ell)}}(\mathbf{y}^{(\ell)}, \zeta^{(\ell)})$ is such that $\mathbf{p}^{(\ell)} = (\mathbf{p}^{(\ell, m)})_{1 \leq m \leq M^{(\ell)}}$, with*

$$\mathbf{p}^{(\ell, m)} = \begin{cases} \mathbf{y}^{(\ell, m)}, & \text{if } |\mathbf{y}^{(\ell, m)}| \leq \tau^{(\ell, m)} \theta^{(\ell)}, \\ \tau^{(\ell, m)} \theta^{(\ell)}, & \text{if } \mathbf{y}^{(\ell, m)} > \tau^{(\ell, m)} \theta^{(\ell)}, \\ -\tau^{(\ell, m)} \theta^{(\ell)}, & \text{if } \mathbf{y}^{(\ell, m)} < -\tau^{(\ell, m)} \theta^{(\ell)}, \end{cases} \quad (42)$$

$$\theta^{(\ell)} = \frac{\max \left(\zeta^{(\ell)} + \sum_{m=\bar{m}^{(\ell)}}^{M^{(\ell)}} \nu^{(\ell, m)} (\tau^{(\ell, m)})^2, 0 \right)}{1 + \sum_{m=\bar{m}^{(\ell)}}^{M^{(\ell)}} (\tau^{(\ell, m)})^2}, \quad (43)$$

and $\bar{m}^{(\ell)}$ is the unique integer in $\{1, \dots, M^{(\ell)} + 1\}$ such that

$$\nu^{(\ell, \bar{m}^{(\ell)}-1)} < \frac{\zeta^{(\ell)} + \sum_{m=\bar{m}^{(\ell)}}^{M^{(\ell)}} \nu^{(\ell, m)} (\tau^{(\ell, m)})^2}{1 + \sum_{m=\bar{m}^{(\ell)}}^{M^{(\ell)}} (\tau^{(\ell, m)})^2} \leq \nu^{(\ell, \bar{m}^{(\ell)})}. \quad (44)$$

Proof. For every $(\mathbf{y}^{(\ell)}, \zeta^{(\ell)}) \in \mathbb{R}^{M^{(\ell)}} \times \mathbb{R}$, in order to determine $P_{\text{epi } h^{(\ell)}}(\mathbf{y}^{(\ell)}, \zeta^{(\ell)})$ we have to find

$$\min_{\theta^{(\ell)} \in [0, +\infty[} \left((\theta^{(\ell)} - \zeta^{(\ell)})^2 + \min_{\substack{|\mathbf{p}^{(\ell, 1)}| \leq \tau^{(\ell, 1)} \theta^{(\ell)} \\ \vdots \\ |\mathbf{p}^{(\ell, M^{(\ell)})}| \leq \tau^{(\ell, M^{(\ell)})} \theta^{(\ell)}}} \|\mathbf{p}^{(\ell)} - \mathbf{y}^{(\ell)}\|^2 \right). \quad (45)$$

For every $\theta^{(\ell)} \in [0, +\infty[$, the inner minimization is achieved when, for every $j \in \{1, \dots, M^{(\ell)}\}$, $\mathbf{p}^{(\ell, m)}$ is the projection of $\mathbf{y}^{(\ell, m)}$ onto $[-\tau^{(\ell, m)} \theta^{(\ell)}, \tau^{(\ell, m)} \theta^{(\ell)}]$, which is given by (42). Then, the problem reduces to

$$\min_{\theta^{(\ell)} \in [0, +\infty[} \left((\theta^{(\ell)} - \zeta^{(\ell)})^2 + \sum_{m=1}^{M^{(\ell)}} (\max\{|\mathbf{y}^{(\ell, m)}| - \tau^{(\ell, m)} \theta^{(\ell)}, 0\})^2 \right) \quad (46)$$

which is also equivalent to calculate $\theta^{(\ell)} = \text{prox}_{\phi^{(\ell)} + \iota_{[0, +\infty[}}(\zeta^{(\ell)})$, where $\phi^{(\ell)}$ is such that, for every $v \in \mathbb{R}$,

$$\phi^{(\ell)}(v) = \frac{1}{2} \sum_{m=1}^{M^{(\ell)}} (\max\{\tau^{(\ell,m)}(\nu^{(\ell,m)} - v), 0\})^2. \quad (47)$$

By using [12, Proposition 12], we have $\text{prox}_{\phi^{(\ell)} + \iota_{[0, +\infty[}} = P_{[0, +\infty[} \circ \text{prox}_{\phi^{(\ell)}}$. The function $\phi^{(\ell)}$ belongs to $\Gamma_0(\mathbb{R})$ since for every $m \in \{1, \dots, M^{(\ell)}\}$, $v \mapsto \max\{\tau^{(\ell,m)}(\nu^{(\ell,m)} - v), 0\}$ is finite convex and $(\cdot)^2$ is finite convex and increasing on $[0, +\infty[$. In addition, $\phi^{(\ell)}$ is differentiable and it is such that, for every $v \in \mathbb{R}$ and every $k \in \{1, \dots, M^{(\ell)} + 1\}$,

$$\nu^{(\ell,k-1)} < v \leq \nu^{(\ell,k)} \quad \Rightarrow \quad \phi^{(\ell)}(v) = \frac{1}{2} \sum_{m=k}^{M^{(\ell)}} (\tau^{(\ell,m)})^2 (v - \nu^{(\ell,m)})^2. \quad (48)$$

For every $\zeta^{(\ell)} \in \mathbb{R}$, as $\chi^{(\ell)} = \text{prox}_{\phi^{(\ell)}}(\zeta^{(\ell)})$ is characterized by (5), there exists $\bar{m}^{(\ell)} \in \{1, \dots, M^{(\ell)} + 1\}$ such that $\nu^{(\ell,\bar{m}^{(\ell)}-1)} < \chi^{(\ell)} \leq \nu^{(\ell,\bar{m}^{(\ell)})}$ and

$$\zeta^{(\ell)} - \chi^{(\ell)} = \sum_{m=\bar{m}^{(\ell)}}^{M^{(\ell)}} (\tau^{(\ell,m)})^2 (\chi^{(\ell)} - \nu^{(\ell,m)}). \quad (49)$$

This yields $\theta^{(\ell)} = P_{[0, +\infty[}(\chi^{(\ell)})$, hence (43), and we have: (44) $\Leftrightarrow \nu^{(\ell,\bar{m}^{(\ell)}-1)} < \chi^{(\ell)} \leq \nu^{(\ell,\bar{m}^{(\ell)})}$. The uniqueness of $\bar{m}^{(\ell)} \in \{1, \dots, M^{(\ell)} + 1\}$ satisfying this inequality follows from the uniqueness of $\text{prox}_{\phi^{(\ell)}}(\zeta^{(\ell)})$. \square

When $\tau^{(\ell,m)} \equiv 1$, the function $h^{(\ell)}$ in (41) reduces to the standard infinity norm $\|\cdot\|_\infty$ for which the expression of the epigraphical projection has been recently given in [?]. Note that this proposition can be employed to efficiently deal with $\ell_{1,\infty}$ regularization which has attracted much interest recently [30, 78, 79].

4 Experimental Results

In this section, we provide numerical examples to illustrate the usefulness of the proposed epigraphical projection method. The first presented experiment focuses on applications in image restoration involving projections onto $\ell_{1,p}$ -balls where $p \in \{2, +\infty\}$. The second experiment deals with a pulse shape design problem based on Proposition 3.4.

4.1 Image restoration

4.1.1 Degradation model

Set $\mathcal{H} = \mathbb{R}^{\bar{N}}$. Denote by $\bar{x} = (\bar{x}^{(n)})_{1 \leq n \leq \bar{N}} \in \mathbb{R}^{\bar{N}}$ the signal of interest, and by $z \in \mathbb{R}^N$ an observation vector such that $z = D\bar{x} + b$. It is assumed that $A \in \mathbb{R}^{\bar{N} \times \bar{N}}$ is a linear operator, $D \in \mathbb{R}^{N \times \bar{N}}$ is

a decimation operator,^{*0} and $b \in \mathbb{R}^N$ is a realization of a zero-mean white Gaussian noise vector. The recovery of \bar{x} from the degraded observations is performed by following a variational approach which aims at solving the following problem

$$\underset{x \in [\underline{\mu}, \bar{\mu}]^{\bar{N}}}{\text{minimize}} \quad \|DAx - z\|^2 \quad \text{s. t.} \quad \sum_{\ell=1}^L \|\Omega_\ell B_\ell F x\|_p \leq \eta, \quad (50)$$

where $(\underline{\mu}, \bar{\mu}) \in \mathbb{R}^2$ with $\underline{\mu} \leq \bar{\mu}$, η is a real positive constant, and $F \in \mathbb{R}^{K \times \bar{N}}$ is the linear operator associated with an analysis transform. Furthermore, for every $\ell \in \{1, \dots, L\}$, $B_\ell \in \mathbb{R}^{M^{(\ell)} \times K}$ is a *block-selection linear operator* which selects a block of $M^{(\ell)}$ data from its input vector.^{*0} For every $\ell \in \{1, \dots, L\}$, Ω_ℓ denotes an $M^{(\ell)} \times M^{(\ell)}$ diagonal matrix of real positive weights.

The term $\|DAx - z\|^2$ is the *data fidelity* corresponding to the negative log-likelihood of x . The bounds $\underline{\mu}$ and $\bar{\mu}$ allow us to take into account the *value range* of each component of \bar{x} . The second constraint involved in Problem (50) promotes solutions having a sparse analysis representation. Indeed, it reduces to the weighted ℓ_1 -norm criterion found in [80] when each block reduces to a singleton (i.e. $L = K$, and, for every $\ell \in \{1, \dots, L\}$, $M^{(\ell)} = 1$ and $B_\ell y = y^{(\ell)}$). It captures the $\ell_{1,2}$ criteria present in [27, 28, 70, 81] when $p = 2$. It matches the $\ell_{1,\infty}$ criterion proposed in [30] when $p = +\infty$.

Note that overlapping blocks in Constraint (50) are dealt with by increasing the dimensionality of the problem (through the linear transform F) and then using an usual non-overlapping block selection operator (denoted B_ℓ). Let us define $\Lambda = [B_1^\top \Omega_1, \dots, B_L^\top \Omega_L]^\top$ and

$$C_1 = \{y \in \mathbb{R}^M \mid \sum_{\ell=1}^L \|y^{(\ell)}\|_p \leq \eta\} \quad (51)$$

where $M = M^{(1)} + \dots + M^{(L)}$ and the same decomposition as in (9) is performed. Then, it can be observed that Problem (50) is a particular case of Problem 1.1 where $S = 2$, $R = 1$, $g_1 = \|D \cdot -z\|^2$, $T_1 = A$, $H_1 = \Lambda F$, C_1 is the above $\ell_{1,p}$ -ball, $H_2 = I$ and $C_2 = [\underline{\mu}, \bar{\mu}]^{\bar{N}}$.

4.1.2 Algorithmic solution

As already mentioned in Section 2.1, various proximal algorithms can be used to solve non-smooth convex optimization problems and would potentially benefit from the proposed epigraphical splitting technique. In this work, we will consider the Monotone+Lipschitz Forward Backward Forward (M+LFBF) algorithm, which is a primal-dual method recently proposed in [60], and the Simultaneous-Direction Method of Multipliers algorithm (SDMM) [2, 66, 82], which is a parallelized version of ADMM. Their convergence is guaranteed (under weak conditions) and their structure makes them suitable for implementation on parallel architectures.

^{*0} D thus corresponds to $N \leq \bar{N}$ lines of the identity $\bar{N} \times \bar{N}$ matrix.

^{*0}This means that there exist distinct indices $m_1, \dots, m_{M^{(\ell)}}$ in $\{1, \dots, K\}$ such that, for every $y = (y^{(k)})_{1 \leq k \leq K} \in \mathbb{R}^K$, $B_\ell y = (y^{(m_j)})_{1 \leq j \leq M^{(\ell)}}$.

Although both algorithms address a wide class of convex optimization problems, SDMM requires to invert the matrix $Q = A^\top A + I + F^\top \Lambda \Lambda F$. This is a well-known limitation of ADMM-like algorithms, which can be circumvented in the case when the matrix Q is diagonalizable in the DFT domain (e.g. see [68, 83]). In the present case, the matrix Q is not diagonalizable since $\Lambda \neq I$. Consequently, SDMM requires to introduce some auxiliary variables into the minimization problem (see [7, 70]) in order to solve the original problem (50). As we will see in Tables 3-4, this makes ADMM-like approaches much slower than primal-dual approaches.

The main difficulty in solving Problem (50) stems from the constraint in (51). The point is that proximal algorithms (as well as most of the applicable algorithms) require to compute the projection onto C_1 . Specific numerical methods [29, 30, 84, 85] have been developed for this purpose. The aim of this section is to propose an alternative method based on the splitting principle presented in Section 3. So doing, the resulting problem can be efficiently addressed by proximal algorithms. The two possible approaches are now detailed.

- *Epigraphical method* – The principle of this method is to decompose C_1 into the closed half-space defined by (12) and the closed convex set defined by (13) with $h^{(\ell)} = \|\cdot\|_p$. We have thus to

$$\underset{(x, \zeta_1) \in C_2 \times V_1}{\text{minimize}} \quad g_1(Ax) \quad \text{s. t.} \quad (\Lambda F x, \zeta_1) \in E_1. \quad (52)$$

The advantage of this decomposition is that the projections onto V_1 and E_1 have closed forms. Indeed, P_{V_1} is the projection onto a half-space, while P_{E_1} is given by Proposition 3.5 for $p = 2$ and Proposition 3.6 for $p = +\infty$. We are then able to solve Problem (52) by means of algorithms such as M+LFBF or SDMM. The associated iterations are given in Algorithm 1. Note that replacing the inequality in the definition of V_1 by an equality constraint $1_{L_1}^\top \zeta_1 = \eta_1$ was observed to make little difference in the numerical behaviour of SDMM.

Algorithm 1 M+LFBF for solving Problem (52)

$$\begin{array}{l} \text{Initialization} \\ \left[\begin{array}{l} (v^{[0]}, \nu^{[0]}) \in \mathbb{R}^M \times \mathbb{R}^L \\ (x^{[0]}, \zeta^{[0]}) \in \mathbb{R}^N \times \mathbb{R}^L \\ \theta = 2\|A\|^2 + \max\{\|\Lambda F\|, 1\} \\ \epsilon \in]0, \frac{1}{\theta+1}[\end{array} \right. \\ \text{For } i = 0, 1, \dots \\ \left[\begin{array}{l} \gamma_i \in \left[\epsilon, \frac{1-\epsilon}{\theta} \right] \\ \left(\hat{x}^{[i]}, \hat{\zeta}^{[i]} \right) = \left(x^{[i]}, \zeta^{[i]} \right) - \gamma_i \left(A^\top \nabla g_1(Ax^{[i]}) + F^\top \Lambda^\top v^{[i]}, \nu^{[i]} \right) \\ \left(p^{[i]}, \rho^{[i]} \right) = P_{C_2 \times V_1} \left(\hat{x}^{[i]}, \hat{\zeta}^{[i]} \right) \\ \left(\hat{v}^{[i]}, \hat{\nu}^{[i]} \right) = \left(v^{[i]}, \nu^{[i]} \right) + \gamma_i \left(\Lambda F x^{[i]}, \zeta^{[i]} \right) \\ \left(a^{[i]}, \alpha^{[i]} \right) = \left(\hat{v}^{[i]}, \hat{\nu}^{[i]} \right) - \gamma_i P_{E_1} \left(\hat{v}^{[i]} / \gamma_i, \hat{\nu}^{[i]} / \gamma_i \right) \\ \left(v^{[i+1]}, \nu^{[i+1]} \right) = \left(a^{[i]}, \alpha^{[i]} \right) + \gamma_i \left(\Lambda F (p^{[i]} - x^{[i]}), \rho^{[i]} - \zeta^{[i]} \right) \\ \left(\tilde{x}^{[i]}, \tilde{\zeta}^{[i]} \right) = \left(p^{[i]}, \rho^{[i]} \right) - \gamma_i \left(A^\top \nabla g_1(Ap^{[i]}) + F^\top \Lambda^\top a^{[i]}, \alpha^{[i]} \right) \\ \left(x^{[i+1]}, \zeta^{[i+1]} \right) = \left(x^{[i]} - \hat{x}^{[i]} + \tilde{x}^{[i]}, \zeta^{[i]} - \hat{\zeta}^{[i]} + \tilde{\zeta}^{[i]} \right) \end{array} \right. \end{array}$$

- *Direct method* – For completeness, we also consider the projection onto C_1 with the algorithm in [29] when $p = 2$,⁰ or the iterative algorithm in [30] when $p = +\infty$.¹ In this case, proximal methods (such as M+LFBF and SDMM) can be used to solve directly Problem (50).

According to the general results in [60, Theorem 4.2] and [2], the sequence $(x^{[i]})_{i \in \mathbb{N}}$ generated by M+LFBF or SDMM is guaranteed to converge to a (global) minimizer of Problem (50).

4.1.3 Smoothness constraint

In the context of image restoration, the quality of the results obtained through a variational approach strongly depends on the ability to model the regularity present in images. Since natural images are often piecewise smooth, popular regularization models tend to penalize the image gradient. In this regard, *total variation* (TV) [27] has emerged as a simple, yet successful, convex optimization tool. However, TV fails to preserve textures, details and fine structures, because they are hardly distinguishable from noise. To improve this behaviour, the TV model has been extended by using a non-locality principle [28, 86]. Another approach to overcome these limitations is to replace the gradient operator with a frame representation which yields a more suitable sparse representation of the image [87]. The connections between these two different approaches have been studied in [88]. It is still unclear which approach leads to the best results. However, there are some evidences that *non-local* (NL) TV may perform better in some image restoration tasks [89, 90, 91]. We thus focus our attention on NLTV-based constraints, although our proposed algorithm is quite general and it can also be adapted to frame-based approaches.

By appropriately selecting the operators F , B_ℓ and Ω_ℓ in Problem (50), we can integrate the NLTV measures in a constrained convex optimization approach. In our experiments, we propose to evaluate the performances of two NLTV constraints that constitute particular cases of the one considered in (50) when $L = \bar{N}$. They are described for 2D data in the following.

- ℓ_2 -NLTV – This constraint has the form

$$\sum_{\ell=1}^{\bar{N}} \left(\sum_{n \in \mathcal{N}_\ell \subset \mathcal{W}_\ell} \omega_{\ell,n} (x^{(\ell)} - x^{(n)})^2 \right)^{1/2} \leq \eta, \quad (53)$$

where \mathcal{N}_ℓ is the *neighbourhood support* at position ℓ and \mathcal{W}_ℓ is the set of positions $n \in \{1, \dots, \bar{N}\} \setminus \{\ell\}$ located into a $Q \times Q$ window centered at ℓ , where $Q \in \mathbb{N}$ is odd. This constraint is a particular case of the one considered in (50) where $K = (Q^2 - 1)\bar{N}$ and F is a concatenation of discrete difference operators F_{q_1, q_2} with $(q_1, q_2) \in \{-(Q-1)/2, \dots, (Q-1)/2\}^2 \setminus \{(0, 0)\}$. More precisely, for every (q_1, q_2) , F_{q_1, q_2} is a 2D filter with impulse response: for every $(n_1, n_2) \in \mathbb{Z}^2$,

$$f_{q_1, q_2}^{(n_1, n_2)} = \begin{cases} 1, & \text{if } n_1 = n_2 = 0, \\ -1, & \text{if } n_1 = q_1 \text{ and } n_2 = q_2, \\ 0, & \text{otherwise.} \end{cases} \quad (54)$$

⁰*Code available at www.cs.ubc.ca/~mpf/spgl1

¹Code available at www.lsi.upc.edu/~aquattoni

In addition, for every $\ell \in \{1, \dots, \bar{N}\}$, $M^{(\ell)} \leq Q^2 - 1$, B_ℓ selects the components of Fx corresponding to differences $(x^{(\ell)} - x^{(n)})_{n \in \mathcal{N}_\ell}$, and the positive weights $(\omega_{\ell,n})_{n \in \mathcal{N}_\ell}$ are gathered in the diagonal matrix Ω_ℓ .

- ℓ_∞ -NLTV– We consider the following constraint

$$\sum_{\ell=1}^{\bar{N}} \max_{n \in \mathcal{N}_\ell} \{\omega_{\ell,n} |x^{(\ell)} - x^{(n)}|\} \leq \eta. \quad (55)$$

We proceed similarly to the previous constraint, except that the ℓ_∞ -norm is now substituted for the ℓ_2 -norm.

Note that the classical isotropic TV constraint (designated by ℓ_2 -TV in the following) constitutes a particular case of the ℓ_2 -NLTV one, where each neighbourhood \mathcal{N}_ℓ only contains the horizontal/vertical neighbouring pixels ($M^{(\ell)} \equiv 2$) and the weights are $\omega_{\ell,n} \equiv 1$. Similarly, the ℓ_∞ -TV constraint is a special case of the ℓ_∞ -NLTV one.

4.1.4 Weight estimation and neighbourhood choice

To set the weights, we got inspired from the Non-Local Means approach originally described in [86]. Here, for every $\ell \in \{1, \dots, \bar{N}\}$ and $n \in \mathcal{N}_\ell$, the weight $\omega_{\ell,n}$ depends on the similarity between patches built around the pixels ℓ and n of the image. Since our degradation process involves some missing data, a two-step approach has been adopted. In the first step, the ℓ_2 -TV approach is used in order to obtain an estimate \tilde{x} of the target image. This estimate is subsequently used in the second step to compute the weights through a *self-similarity* measure, yielding

$$\omega_{\ell,n} = \tilde{\omega}_\ell \exp \left(-\delta^{-2} \|\tilde{B}_\ell \tilde{F}_\ell \tilde{x} - \tilde{B}_n \tilde{F}_n \tilde{x}\|^2 \right), \quad (56)$$

where $\delta \in \mathbb{R} \setminus \{0\}$, $\tilde{\omega}_\ell \in]0, +\infty[$, \tilde{B}_ℓ (resp. \tilde{B}_n) selects a $\tilde{Q} \times \tilde{Q}$ patch centered at position ℓ (resp. n) and \tilde{F}_ℓ (resp. \tilde{F}_n) is a linear processing of the image depending on the position ℓ (resp. n). The constant $\tilde{\omega}_\ell$ is set so as to normalize the weights (i.e. $\sum_{n \in \mathcal{N}_\ell} \omega_{\ell,n} = 1$).

The measure in (56) generalizes the one proposed in [86], which corresponds to the case when \tilde{F}_ℓ (resp. \tilde{F}_n) reduces to a Gaussian function with mean ℓ (resp. n). In the present work, we consider the *foveated self-similarity* measure recently introduced in [92], due to its better performance in denoising. This approach can be derived from (56) by setting \tilde{F}_ℓ (resp. \tilde{F}_n) to a set of low-pass Gaussian filters whose variances increase as the spatial distance from the patch center ℓ (resp. n) grows.

For every $\ell \in \{1, \dots, \bar{N}\}$, the neighbourhood \mathcal{N}_ℓ is built according to the procedure described in [93]. In practice, we limit the size of the neighbourhood, so that $M^{(\ell)} \leq \bar{M}$ (a possible choice of \bar{M} is given in the next paragraph).

4.1.5 Numerical results – analysis of convergence times

In this section, the execution time of the proposed epigraphical technique is evaluated w.r.t. the direct method involving standard numerical solutions.

In the following experiments, if not specified otherwise, the degradation matrix A is a convolution which consists of a 3×3 uniform blur and the decimation matrix D randomly removes 60% of the pixels ($N = 0.4 \times \bar{N}$). The standard deviation of the additive white Gaussian noise is equal to $\sigma = 10$. Since we deal with natural images, the data range bounds are $\underline{\mu} = 0$ and $\bar{\mu} = 255$. For the smoothness constraint, we set $Q = 11$, $\tilde{Q} = 5$, $\delta = 35$ and $\bar{M} = 14$.

We present the results obtained with the image *boat* cropped at 256×256 ($\bar{N} = 256^2$), since a similar behaviour was observed for other images. The stopping criterion is set to $\|x^{[i+1]} - x^{[i]}\| \leq 10^{-4} \|x^{[i]}\|$. For the $\ell_{1,p}$ -ball projectors needed by the direct method, we used the software publicly available on-line [29, 30].

Note that SDMM requires to invert the matrix $Q = A^\top A + I + F^\top \Lambda \Lambda F$, which we address by resorting to the solution proposed in [7, 70]. In order to make the operators A and F diagonalizable in the DFT domain, a periodic extension of the image is performed.

In practice, the constraint bound η may not be known precisely. Although it is out of the scope of this paper to devise an optimal strategy to set this bound, it is important to evaluate the impact of its choice on our method performance. In the following, we compare the epigraphical approach with the direct computation of the projections (via standard iterative solutions) for different choices of regularization constraints and values of η .

- *Total Variation* – Tables 1 and 2 report a comparison between the direct and epigraphical methods for ℓ_2 -TV and ℓ_∞ -TV, respectively. For more readability, the values of η are expressed as a multiplicative factor of the ℓ_p -TV-semi-norm of the original image. The convergence times indicate that the epigraphical approach yields a faster convergence than the direct approach for SDMM and M+LFBF. Moreover, the numerical results show that errors within $\pm 20\%$ from the optimal value for η lead to SNR variations within 2%.

Figs. 1-a and 1-b show the relative error $\|x^{[i]} - x^{[\infty]}\| / \|x^{[\infty]}\|$ as a function of the computational time, where $x^{[\infty]}$ denotes the solution computed after a large number of iterations (typically, 5000 iterations). The dashed line presents the results for the direct method while the solid line refers to the epigraphical one. These plots show that the epigraphical approach is faster despite it requires more iterations in order to converge. This can be explained by the computational cost of the subiterations required by the direct projections onto the $\ell_{1,p}$ -ball.

- ℓ_2 -NLTV – Table 3 collects the results of ℓ_2 -NLTV for different values of neighbourhood size Q . To set the weights, the first TV estimate is computed with $\eta = 0.56$. The convergence times show that the epigraphical approach is faster than the direct one for both considered algorithms. Moreover, it can be noticed that errors within $\pm 20\%$ from the optimal bound value lead to SNR variations within 1%. In Figure 1-c, a plot similar to those in Figs. 1-a and 1-b show the convergence profile. The epigraphical method requires about the same number

Table 1: Results for the ℓ_2 -TV constraint and different values of η

η	SNR (dB) – SSIM	SDMM					M+LFBF				
		direct		epigraphical		speed up	direct		epigraphical		speed up
		# iter.	sec.	# iter.	sec.		# iter.	sec.	# iter.	sec.	
0.45	19.90 – 0.733	107	6.07	174	2.03	2.99	113	6.15	182	3.49	1.76
0.50	20.18 – 0.745	117	6.95	159	1.95	3.57	116	6.97	168	3.44	2.03
0.56	20.23 – 0.745	129	8.36	153	1.90	4.41	124	8.17	159	3.01	2.72
0.62	20.16 – 0.737	141	9.44	155	1.83	5.16	131	8.62	159	3.26	2.65
0.67	20.00 – 0.724	154	10.20	162	2.17	4.71	140	10.00	164	2.84	3.52

Table 2: Results for the ℓ_∞ -TV constraint and different values of η

η	SNR (dB) – SSIM	SDMM					M+LFBF				
		direct		epigraphical		speed up	direct		epigraphical		speed up
		# iter.	sec.	# iter.	sec.		# iter.	sec.	# iter.	sec.	
0.45	19.52 – 0.726	160	312.55	231	3.89	80.43	183	347.10	252	6.43	53.96
0.50	19.71 – 0.734	168	342.01	215	3.75	91.31	185	368.24	236	5.83	63.17
0.56	19.71 – 0.728	180	373.60	211	3.49	106.93	189	386.29	229	5.53	69.91
0.62	19.59 – 0.715	196	412.68	216	3.67	112.50	198	411.04	229	5.86	70.15
0.67	19.39 – 0.698	211	448.77	223	3.76	119.27	207	437.66	234	5.76	75.96

Table 3: Results for the ℓ_2 -NLTV constraint and some values of η and Q

η	SNR (dB) – SSIM	SDMM					M+LFBF				
		direct		epigraphical		speed up	direct		epigraphical		speed up
		# iter.	sec.	# iter.	sec.		# iter.	sec.	# iter.	sec.	
Neighbourhood size: $Q = 3$											
0.43	20.82 – 0.757	208	20.67	211	10.93	1.89	82	6.95	93	3.76	1.85
0.49	20.97 – 0.765	167	16.84	177	9.01	1.87	75	6.61	83	3.47	1.91
0.54	21.02 – 0.767	147	15.31	157	7.93	1.93	71	6.45	77	3.15	2.04
0.59	20.98 – 0.764	134	14.44	148	7.67	1.88	72	6.58	77	3.24	2.03
0.65	20.88 – 0.757	133	14.82	136	7.11	2.08	76	7.53	80	3.27	2.30
Neighbourhood size: $Q = 5$											
0.43	21.00 – 0.766	301	56.03	343	45.18	1.24	82	8.51	90	5.43	1.57
0.49	21.15 – 0.773	260	49.03	302	39.64	1.24	75	7.90	81	4.90	1.61
0.54	21.20 – 0.775	242	46.31	283	37.72	1.23	71	8.26	75	4.47	1.85
0.59	21.17 – 0.773	231	46.20	268	36.56	1.26	70	7.94	74	4.49	1.77
0.65	21.08 – 0.767	220	44.64	252	34.46	1.30	73	8.40	76	4.59	1.83

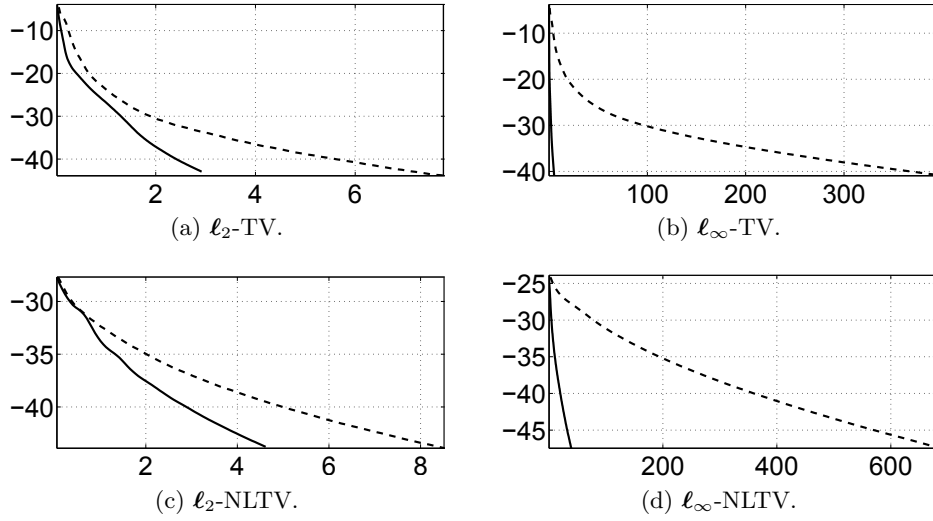


Figure 1: Comparison between epigraphical method (*solid line*) and direct method (*dashed line*): $\frac{\|x^{[i]} - x^{[\infty]}\|}{\|x^{[\infty]}\|}$ in dB vs time

of iterations as the direct one in order to converge. This results in a time reduction, as a single iteration of the epigraphical method is faster than one iteration of the direct method.

- ℓ_∞ -NLTV – Table 4 and Figure 1-d show the results obtained with the ℓ_∞ -NLTV constraint. Similarly to ℓ_∞ -TV, the epigraphical approach greatly speeds up the convergence times.

4.1.6 Numerical results – restoration performance

In this section, the quality of images reconstructed with our variational approach is evaluated for different choices of regularization constraints and comparisons are made with a state-of-the-art method. Extensive tests have been carried out on several standard images of different sizes. The SNR and SSIM [94] results obtained by using the various previously introduced TV-like constraints are collected in Table 5. In addition, a comparison is performed between our method using an M+LFBF implementation and the Gradient Projection for Sparse Reconstruction (GPSR) method [51], which also relies on a variational approach. The constraint bound for both methods was hand-tuned in order to achieve the best SNR values. The best results are highlighted in bold. A visual comparison is made in Figure 2, where two representative images are displayed. These results demonstrate the interest of considering non-local smoothness measures. Indeed, NLTV with $\ell_{1,2}$ -norm proves to be the most effective constraint with gains in SNR and SSIM (up to 1.82 dB and 0.042) with respect to ℓ_2 -TV, which in turn outperforms GPSR. The better performance of NLTV seems to be related to its ability to better preserve edges and thin structures present in images. In terms of computational time, GPSR is about twice faster than ℓ_2 -NLTV. Our codes were developed in MATLAB^{* 0}, the operators F and F^\top being implemented in C using mex files.

⁰*R2011b version on an Intel Xeon CPU at 2.80 GHz and 8 GB of RAM.

In order to complete the analysis, we report in Figure 3 SNR/SSIM comparisons between ℓ_2 -NLTV and ℓ_2 -TV for different blur and noise configurations. These plots show that ℓ_2 -NLTV provides better results regardless of the degradation conditions.

4.2 Pulse shape design

4.2.1 Problem

We consider a pulse shape design problem for digital communications. This problem has been previously addressed in terms of constrained optimization in [13, 95, 96]. Based on the epigraphical approach, we are able to revisit this problem by relaxing some of the involved constraints.

Five constraints arise from engineering specifications [13]. We denote by $x = (x^{(k)})_{0 \leq k \leq N-1} \in \mathbb{R}^N$ the pulse and by $\chi = (\chi^{(k)})_{0 \leq k \leq N-1}$ its discrete Fourier transform. The underlying sampling rate is 2560 Hz and the involved constraints are:

- (i) Bound on the modulus of χ . The modulus of the Fourier transform should not exceed a prescribed bound $\gamma = 10^{-3/2}$ beyond 300 Hz. This leads to

$$(\forall k \in \mathbb{D}_1) \quad C_1^{(k)} = \{x \in \mathbb{R}^N \mid |\chi^{(k)}| \leq \gamma\} \quad (57)$$

where \mathbb{D}_1 represents frequencies beyond 300 Hz.

- (ii) Vanishing frequencies of χ at the zero frequency and at integer multiples of 50 Hz:

$$C_2 = \{x \in \mathbb{R}^N \mid (\forall k \in \mathbb{D}_2) \chi^{(k)} = 0\} \quad (58)$$

where \mathbb{D}_2 denotes frequencies where the Fourier transform χ vanishes.

- (iii) Pulse energy should not exceed a bound $\mu > 0$ (in order to avoid interference with other systems):

$$C_3 = \{x \in \mathbb{R}^N \mid \|x\| \leq \mu\}. \quad (59)$$

- (iv) Symmetry of the pulse and its mid-point value should be equal to 1:

$$C_4 = \{x \in \mathbb{R}^N \mid x^{(N/2)} = 1 \text{ and } (\forall k \in \{0, \dots, N/2\}) x^{(k)} = x^{(N-1-k)}\}. \quad (60)$$

- (v) Pulse duration should be 50 ms and it should have periodic zero crossings every 3.125 ms:

$$C_5 = \{x \in \mathbb{R}^N \mid (\forall k \in \mathbb{D}_3) x^{(k)} = 0\} \quad (61)$$

where \mathbb{D}_3 is the set of time indices in the zero areas.

Some of the above constraints (e.g. the second and the last ones) are incompatible and, in order to make the problem feasible, we propose to replace the constraint sets $(C_1^{(k)})_{1 \leq k \leq N}$ with

$$C_1 = \{x \in \mathbb{R}^N \mid \sum_{k \in \mathbb{D}_1} d_{C_1^{(k)}}^\beta(\chi^{(k)}) \leq \varepsilon\} \quad (62)$$

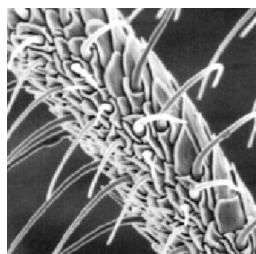
where $\varepsilon > 0$ and $\beta \in [1, +\infty[$.

Table 4: Results for the ℓ_∞ -NLTV constraint and some values of η and Q

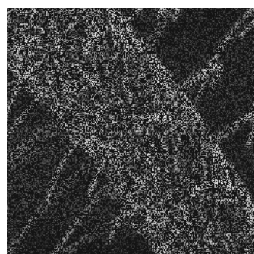
η	SNR (dB) – SSIM	SDMM					M+LFBF				
		direct		epigraphical		speed up	direct		epigraphical		speed up
		# iter.	sec.	# iter.	sec.		# iter.	sec.	# iter.	sec.	
Neighbourhood size: $Q = 3$											
0.43	20.78 – 0.762	434	1470.46	449	25.03	58.76	225	730.26	244	12.35	59.15
0.49	20.86 – 0.764	395	1319.64	413	22.86	57.72	221	692.25	237	11.92	58.08
0.54	20.83 – 0.760	363	1193.61	382	21.46	55.62	217	667.50	233	11.46	58.22
0.59	20.73 – 0.752	340	1093.26	354	19.77	55.30	216	653.79	230	11.67	56.01
0.65	20.58 – 0.740	322	1007.55	336	18.64	54.06	216	643.00	229	11.45	56.18
Neighbourhood size: $Q = 5$											
0.43	20.91 – 0.769	384	2069.62	452	64.42	32.13	233	863.01	252	18.47	46.73
0.49	20.98 – 0.771	326	1700.34	412	58.66	28.99	231	822.06	247	18.36	44.77
0.54	20.97 – 0.767	290	1476.98	389	55.35	26.69	229	787.61	245	17.90	43.99
0.59	20.88 – 0.759	276	1336.16	374	52.64	25.38	230	772.42	245	17.57	43.96
0.65	20.75 – 0.749	268	1220.14	362	51.45	23.72	231	760.86	245	17.81	42.72

Table 5: SNR_{dB} and SSIM results of our method and GPSR (noise parameters: blur = 3×3 , $\sigma = 10$, decimation = 60%)

SNR (dB) – SSIM	\bar{N}	ℓ_2 -TV	ℓ_∞ -TV	ℓ_2 -NLTV	ℓ_∞ -NLTV	GPSR
CULICOIDAE	256 ²	20.80 – 0.855	20.25 – 0.853	22.62 – 0.897	22.38 – 0.897	17.03 – 0.738
LENA	256 ²	23.18 – 0.783	22.77 – 0.769	24.18 – 0.812	24.14 – 0.812	20.26 – 0.678
BOAT	256 ²	20.25 – 0.739	19.74 – 0.718	21.13 – 0.770	20.77 – 0.741	18.06 – 0.649
CAMERAMAN	256 ²	20.06 – 0.774	19.68 – 0.755	20.71 – 0.801	20.17 – 0.743	17.92 – 0.673
HOUSE	256 ²	25.47 – 0.823	24.70 – 0.808	26.31 – 0.836	25.87 – 0.823	22.14 – 0.734
MAN	256 ²	19.24 – 0.725	18.96 – 0.714	19.66 – 0.741	19.51 – 0.736	17.11 – 0.629
PEPPERS	512 ²	23.69 – 0.801	23.25 – 0.786	24.80 – 0.829	24.45 – 0.813	21.94 – 0.709
BARBARA	512 ²	16.74 – 0.653	16.64 – 0.642	17.02 – 0.673	16.99 – 0.652	15.97 – 0.562
HILL	512 ²	22.18 – 0.723	21.89 – 0.715	22.55 – 0.735	22.43 – 0.733	20.21 – 0.637
CULICOIDAE	1024 ²	20.84 – 0.855	20.49 – 0.812	23.25 – 0.885	22.57 – 0.810	17.19 – 0.725



(a) Culicoidae.



(b) Degraded.



(c) Zoom.



(d) GPSR,
SNR: 17.03 dB.



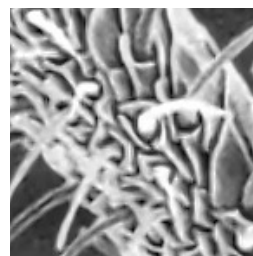
(e) ℓ_2 -TV,
SNR: 20.80 dB.



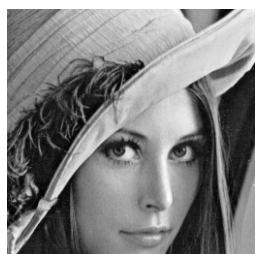
(f) ℓ_∞ -TV,
SNR: 20.25 dB.



(g) ℓ_2 -NLTV,
SNR: **22.62 dB.**



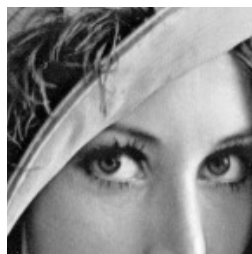
(h) ℓ_∞ -NLTV,
SNR: 22.38 dB.



(i) Lena.



(j) Degraded.



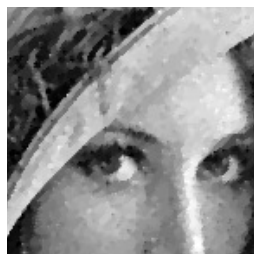
(k) Zoom.



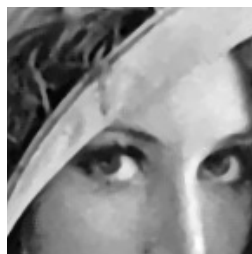
(l) GPSR,
SNR: 20.26 dB.



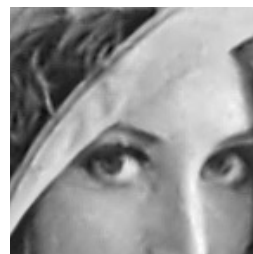
(m) ℓ_2 -TV,
SNR: 23.18 dB.



(n) ℓ_∞ -TV,
SNR: 22.77 dB.



(o) ℓ_2 -NLTV,
SNR: **24.18 dB.**



(p) ℓ_∞ -NLTV,
SNR: 24.14 dB.

Figure 2: Image restoration examples (noise parameters: blur = 3×3 , $\sigma = 10$, decimation = 60%)

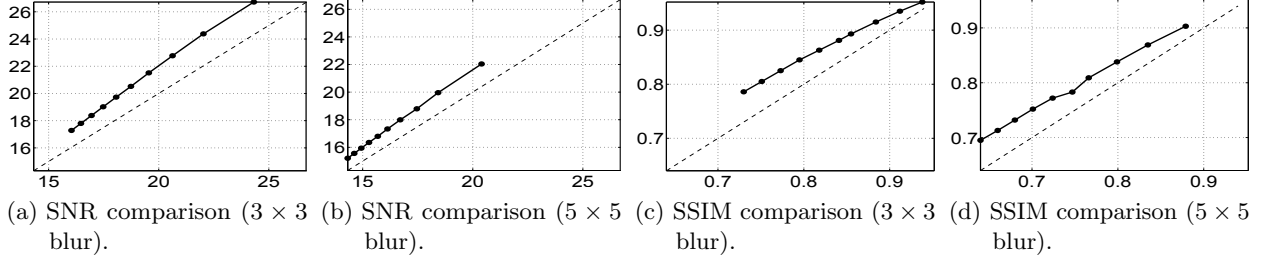


Figure 3: SNR and SSIM values for ℓ_2 -NLTV (vertical axes) and ℓ_2 -TV (horizontal axes), for the *culicoidae* image. The plots show the results obtained for $\sigma \in \{5, 10, \dots, 50\}$, where lower SNR or SSIM values correspond to higher σ values. No decimation is applied in this experiment.

4.2.2 Algorithmic solution

The resulting optimization problem reads

$$\underset{x \in \mathbb{R}^N}{\text{minimize}} \quad \|x\|^2 + \sum_{s=1}^5 \iota_{C_s}(x). \quad (63)$$

A squared ℓ_2 -norm has been included in the criterion in order to ensure the uniqueness of the solution. Algorithms usually employed for solving such a kind of problem [13] require closed form expressions of the projection associated with each involved constraint. The projections onto C_2 , C_4 , and C_5 are standard projections onto vector subspaces. The projection onto C_3 is the projection onto an ℓ_2 -ball which also has a closed form. The difficulty stems from the computation of the projection onto the convex set C_1 . We propose to split it into two constraints as proposed in Section 3. More specifically, Problem (63) can be equivalently written as

$$\underset{(x, \zeta_1) \in \mathbb{R}^N \times V_1}{\text{minimize}} \quad \|x\|^2 + \iota_{E_1}(x, \zeta_1) + \sum_{s=2}^5 \iota_{C_s}(x) \quad (64)$$

where

$$V_1 = \{\zeta \in \mathbb{R}^N \mid \mathbf{1}_{\mathbb{D}_1}^\top \zeta \leq \varepsilon\} \quad (65)$$

and the closed convex set E is

$$E_1 = \{(x, \zeta) \in \mathbb{R}^N \times \mathbb{R}^N \mid (\forall k \in \mathbb{D}_1) \, d_{C_1^{(k)}}^\beta(x) \leq \zeta^{(k)}\}. \quad (66)$$

The projection onto V_1 is well-known [36], while the projection onto E_1 follows from Proposition 3.4.

4.2.3 Numerical results

Several experiments are performed in order to compare state-of-the-art solutions with the proposed constrained formulation. The results are summarized in Figs 4 and 6. Fig. 4 presents state-of-the-art

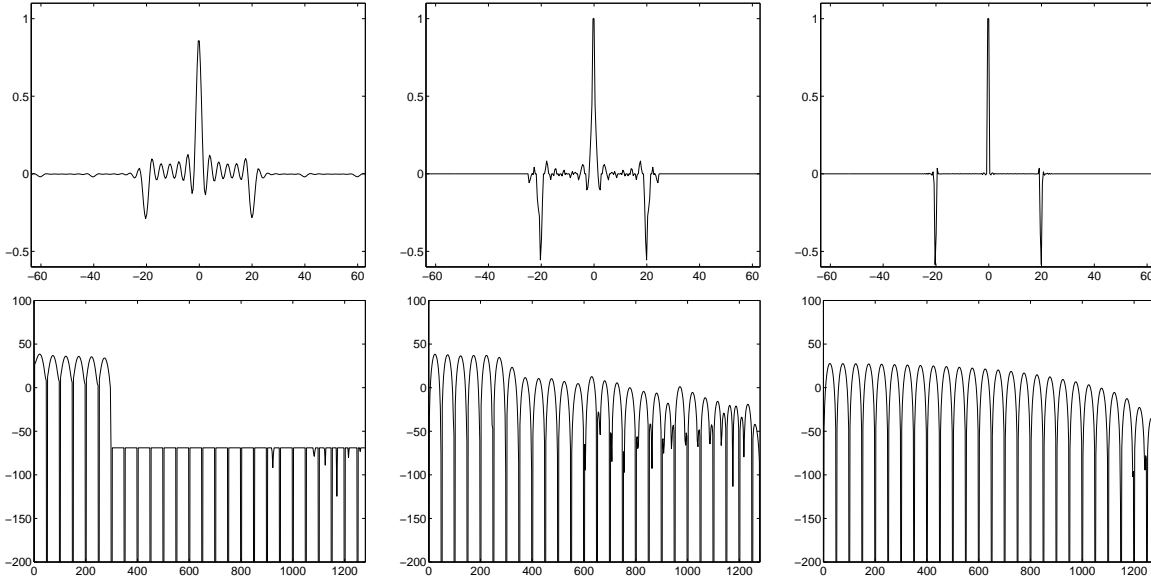


Figure 4: State-of-the-art results. First row: pulse x , second row: Fourier transform χ of the pulse. The results in the first column are obtained by minimizing $d_{C_4}(x) + d_{C_5}(x)$ subject to $x \in \left(\bigcap_{k \in \mathbb{D}_1} C_1^k\right) \cap (C_2 \cap C_3)$, the results in the second one are obtained by minimizing $\sum_{k \in \mathbb{D}_1} d_{C_1^k}^2(x)$ subject to $x \in C_2 \cap C_3 \cap C_4 \cap C_5$, and the last one presents a solution in $C_2 \cap C_3 \cap C_4 \cap C_5$.

results (from [13]). Fig. 5 shows the results obtained with the proposed solution for $\beta = 1$ and different values of ε leading to admissible solutions while Fig. 6 presents admissible solutions for $\beta = 2$ and different values of ε . Note that for large values of ε , the solutions for $\beta = 1$ or $\beta = 2$ converge to a solution of the unconstrained (without imposing C_1) problem (cf. Fig 4-right). For $\beta = 2$, it is also interesting to experimentally observe that the estimated pulse for the smallest value of ε leading an admissible solution (cf. Fig 6-left) is similar to the solution proposed in [13] (cf. Fig. 4 - middle).

As illustrated by these experiments, the proposed approach allows us to gain more design flexibility at the expense of a small additional computational cost.

5 Conclusions

We have proposed a new epigraphical technique to deal with constrained convex variational formulations of inverse problems with the help of proximal algorithms. In this paper, our attention has been turned to constraints based on distance functions and weighted $\ell_{1,p}$ -norms with $p \in \{2, +\infty\}$. In the context of 1D signals, we have shown that constraints based on distance functions are useful for pulse shape design. In the context of images, we have used $\ell_{1,p}$ -norm constraints to promote block-sparsity of analysis representations. The obtained results demonstrate the better performance of non-local measures in terms of image quality. Our results also show that the $\ell_{1,2}$ -norm has to be preferred over the $\ell_{1,\infty}$ -norm for image recovery problems. However, it would

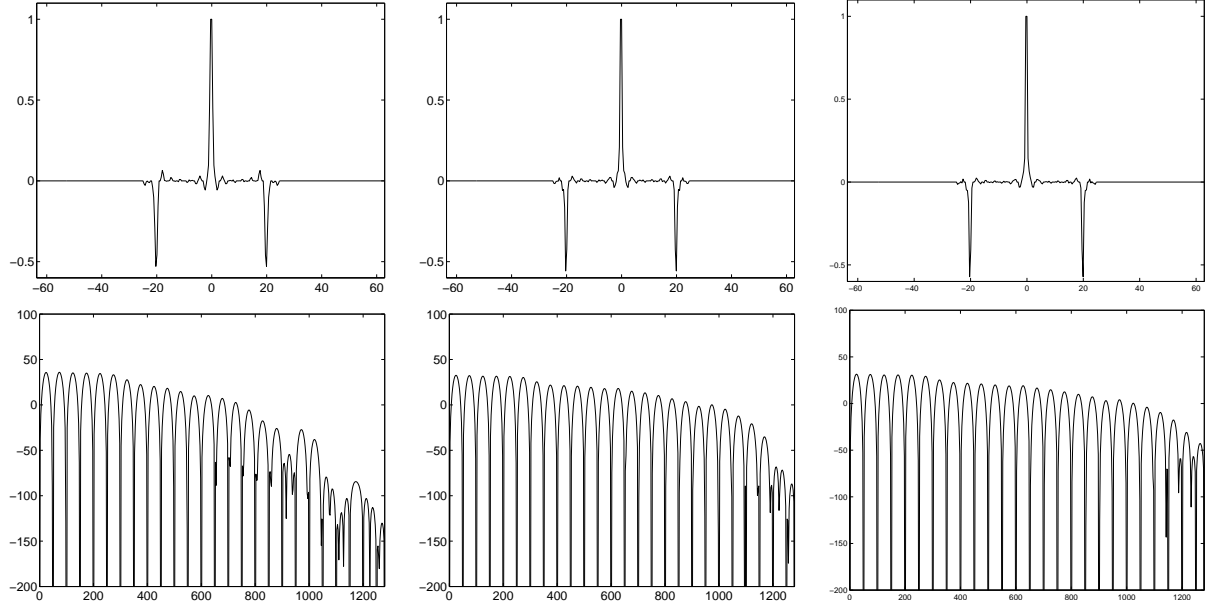


Figure 5: Results obtained from (64) for $\beta = 1$ and $\epsilon = 800$ (first column), $\epsilon = 1000$ (second column), and $\epsilon = 2000$ (third column). First row: pulse x , second row: Fourier transform χ of the pulse.

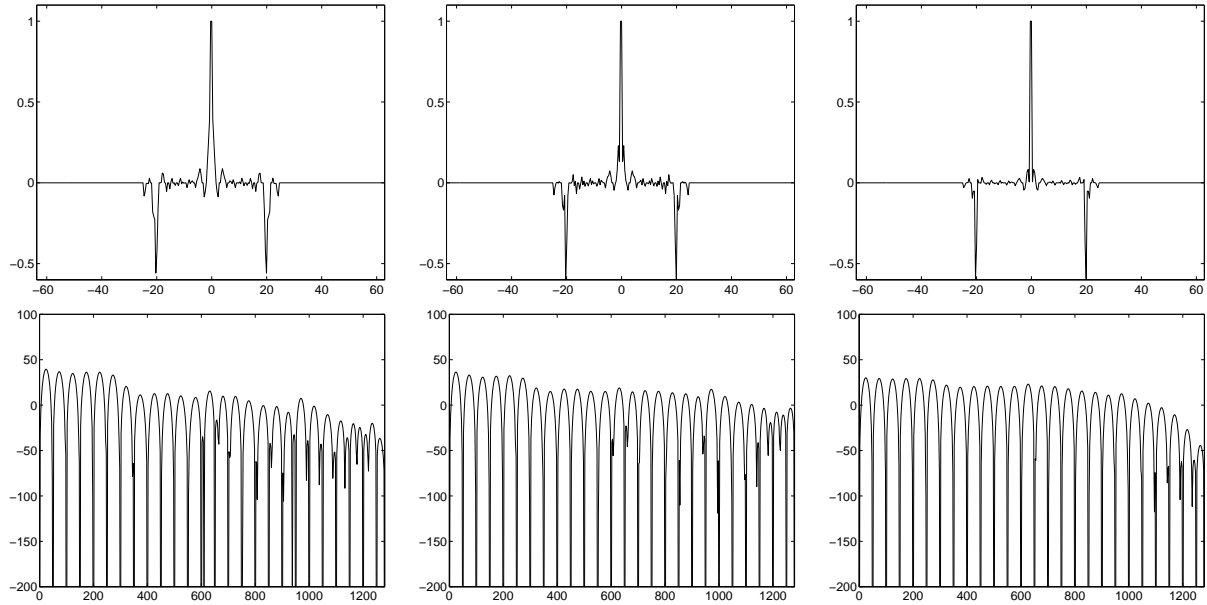


Figure 6: Results obtained from (64) for $\beta = 2$ and $\epsilon = 800$ (first column), $\epsilon = 5000$ (second column), $\epsilon = 10000$ (third column). First row: pulse x , second row: Fourier transform χ of the pulse.

be interesting to consider alternative applications of $\ell_{1,\infty}$ -norms such as regression problems [97,98]. Furthermore, the experimental part indicates that the epigraphical method converges faster than the approach based on the direct computation of the projections via standard iterative solutions. Parallelization of our codes should even allow us to accelerate them [99]. Note that, although the considered application involves two constraint sets, the proposed approach can handle an arbitrary number of convex constraints. The epigraphical approach could also be used to develop approximation methods for addressing more general convex constraints.

References

References

- [1] R. T. Rockafellar. Monotone operators and the proximal point algorithm. *SIAM J. Control Optim.*, 14:877–898, 1976.
- [2] P. L. Combettes and J.-C. Pesquet. Proximal splitting methods in signal processing. In H. H. Bauschke, R. S. Burachik, P. L. Combettes, V. Elser, D. R. Luke, and H. Wolkowicz, editors, *Fixed-Point Algorithms for Inverse Problems in Science and Engineering*, pages 185–212. Springer-Verlag, New York, 2011.
- [3] F. Bach, R. Jenatton, J. Mairal, and G. Obozinski. Optimization with sparsity-inducing penalties. *Foundations and Trends in Machine Learning*, 4(1):1–106, 2012.
- [4] M. Guerquin-Kern, M. Häberlin, K.P. Pruessmann, and M. Unser. A fast wavelet-based reconstruction method for magnetic resonance imaging. *IEEE Trans. Med. Imag.*, 30(9):1649–1660, Sep. 2011.
- [5] F.-X. Dupé, M. J. Fadili, and J.-L. Starck. A proximal iteration for deconvolving Poisson noisy images using sparse representations. *IEEE Trans. Image Process.*, 18(2):310–321, Feb. 2009.
- [6] J.-F. Aujol, G. Gilboa, T. Chan, and S. Osher. Structure-texture image decomposition - modeling, algorithms, and parameter selection. *Int. J. Comp. Vis.*, 67(1):111–136, Apr. 2006.
- [7] L. M. Briceño-Arias, P. L. Combettes, J.-C. Pesquet, and N. Pustelnik. Proximal algorithms for multicomponent image recovery problems. *J. Math. Imag. Vis.*, 41(1):3–22, Sep. 2011.
- [8] S. Theodoridis, K. Slavakis, and I. Yamada. Adaptive learning in a world of projections. *IEEE Signal Process. Mag.*, 28(1):97–123, Jan. 2011.
- [9] C. Chaux, M. El Gheche, J. Farah, J.-C. Pesquet, and B. Pesquet-Popescu. A parallel proximal splitting method for disparity estimation from multicomponent images under illumination variation. *J. Math. Imag. Vis.*, 47(3):167–178, November 2013.
- [10] P. L. Combettes and V. R. Wajs. Signal recovery by proximal forward-backward splitting. *Multiscale Model. and Simul.*, 4(4):1168–1200, Nov. 2005.

- [11] C. Chaux, P. L. Combettes, J.-C. Pesquet, and V. R. Wajs. A variational formulation for frame-based inverse problems. *Inverse Problems*, 23(4):1495–1518, Jun. 2007.
- [12] P. L. Combettes and J.-C. Pesquet. A Douglas-Rachford splitting approach to nonsmooth convex variational signal recovery. *IEEE J. Selected Topics Signal Process.*, 1(4):564–574, Dec. 2007.
- [13] P. L. Combettes and J.-C. Pesquet. A proximal decomposition method for solving convex variational inverse problems. *Inverse Problems*, 24(6), Dec. 2008.
- [14] N. P. Galatsanos and A. K. Katsaggelos. Methods for choosing the regularization parameter and estimating the noise variance in image restoration and their relation. *IEEE Trans. Image Process.*, 1(3):322–336, Jul. 1992.
- [15] P. C. Hansen and D. P. O’Leary. The use of the L-curve in the regularization of discrete ill-posed problems. *SIAM J. Sci. Comput.*, 14(6):1487–1503, 1993.
- [16] A. Pizurica and W. Philips. Estimating the probability of the presence of a signal of interest in multiresolution single- and multiband image denoising. *IEEE Trans. Image Process.*, 15(3):654–665, Mar. 2006.
- [17] S. Ramani, T. Blu, and M. Unser. Monte-Carlo SURE: A black-box optimization of regularization parameters for general denoising algorithms. *IEEE Trans. Image Process.*, 17(9):1540–1554, Sep. 2008.
- [18] L. Chaari, J.-C. Pesquet, J.-Y. Tournet, P. Ciuciu, and A. Benazza-Benyahia. A hierarchical bayesian model for frame representation. *IEEE Trans. Signal Process.*, 58(11):5560–5571, Nov. 2010.
- [19] D. C. Youla and H. Webb. Image restoration by the method of convex projections. Part I - theory. *IEEE Trans. Med. Imag.*, 1(2):81–94, Oct. 1982.
- [20] H. J. Trussell and M. R. Civanlar. The feasible solution in signal restoration. *IEEE Trans. Acous., Speech Signal Process.*, 32(2):201–212, Apr. 1984.
- [21] P. L. Combettes. Inconsistent signal feasibility problems : least-squares solutions in a product space. *IEEE Trans. Signal Process.*, 42(11):2955–2966, Nov. 1994.
- [22] K. Kose, V. Cevher, and A. E. Cetin. Filtered variation method for denoising and sparse signal processing. In *Proc. Int. Conf. Acoust., Speech Signal Process.*, Kyoto, Japan, March, 27-30 2012.
- [23] T. Teuber, G. Steidl, and R. H. Chan. Minimization and parameter estimation for seminorm regularization models with I-divergence constraints. *Inverse Problems*, 29:x+29, 2013.
- [24] R. Stück, M. Burger, and T. Hohage. The iteratively regularized Gauss-Newton method with convex constraints and applications in 4Pi microscopy. *Inverse Problems*, 28:x+17, 2012.
- [25] S. Ono and I. Yamada. Poisson image restoration with likelihood constraint via hybrid steepest descent method. In *Proc. Int. Conf. Acoust., Speech Signal Process.*, pages x+5, Vancouver, Canada, May 26 - 31 2013.

- [26] R. Ciak, B. Shafei, and G. Steidl. Homogeneous penalizers and constraints in convex image restoration. *J. Math. Imag. Vis.*, 2012.
- [27] L. Rudin, S. Osher, and E. Fatemi. Nonlinear total variation based noise removal algorithms. *Physica D*, 60(1-4):259–268, Nov. 1992.
- [28] G. Gilboa and S. Osher. Nonlocal Operators with Applications to Image Processing. *Multiscale Model. and Simul.*, 7(3):1005, 2009.
- [29] E. Van Den Berg and M. P. Friedlander. Probing the Pareto frontier for basis pursuit solutions. *SIAM J. Sci. Comput.*, 31(2):890–912, Nov. 2008.
- [30] A. Quattoni, X. Carreras, M. Collins, and T. Darrell. An efficient projection for $\ell_{1,\infty}$ regularization. In *International Conference on Machine Learning*, Montreal, Quebec, Jun., 14-18 2009.
- [31] A. Tikhonov. Tikhonov regularization of incorrectly posed problems. *Soviet Mathematics Doklady*, 4:1624–1627, 1963.
- [32] E. Chouzenoux, J. Idier, and S. Moussaoui. A Majorize-Minimize strategy for subspace optimization applied to image restoration. *IEEE Trans. Image Process.*, 20(6):1517–1528, Jun. 2011.
- [33] B. Martinet. Régularisation d’inéquations variationnelles par approximations successives. *Informat. Recherche Opérationnelle*, 4:154–158, 1970.
- [34] G. Aubert and R. Tahraoui. Sur la minimisation d’une fonctionnelle non convexe, non différentiable en dimension 1. *Bolletino UMI*, 5(17B), 1980.
- [35] A. Ben-Tal and M. Teboulle. A smoothing technique for nondifferentiable optimization problems. *Lecture Notes in Mathematics*, 1405:1–11, 1989.
- [36] J.-B. Hiriart-Urruty and C. Lemaréchal. *Convex analysis and minimization algorithms, Part I : Fundamentals*, volume 305 of *Grundlehren der mathematischen Wissenschaften*. Springer-Verlag, Berlin, Heidelberg, N.Y., 2nd edition, 1996.
- [37] P. Tseng. Convergence of a block coordinate descent method for nondifferentiable minimization. *Journal of Opt. Theory and Applications*, 109(3):475–494, Jun. 2001.
- [38] S. J. Wright. *Primal-dual interior-point methods*. SIAM, Philadelphia, PA, 1997.
- [39] L. M. Bregman. The method of successive projection for finding a common point of convex sets. *Soviet Math. Dokl.*, 6:688–692, 1965.
- [40] L. G. Gurin, B. T. Polyak, and E. V. Raik. Projection methods for finding a common point of convex sets. *Zh. Vychisl. Mat. Mat. Fiz.*, 7(6):1211–1228, 1967.
- [41] P. L. Combettes. The foundations of set theoretic estimation. *Proceedings of the IEEE*, 81(2):182–208, Feb. 1993.

- [42] P. L. Combettes. Convex set theoretic image recovery by extrapolated iterations of parallel subgradient projections. *IEEE Trans. Image Process.*, 6(4):492–506, Apr. 1997.
- [43] Y. Censor, W. Chen, P. L. Combettes, R. Davidi, and G. T. Herman. On the effectiveness of projection methods for convex feasibility problems with linear inequality constraints. *Comput. Optim. Appl.*, 51(3):1065–1088, 2012.
- [44] H. H. Bauschke and P. L. Combettes. *Convex Analysis and Monotone Operator Theory in Hilbert Spaces*. Springer, New York, 2011.
- [45] P. L. Combettes. A block-iterative surrogate constraint splitting method for quadratic signal recovery. *IEEE Trans. Signal Process.*, 51(7):1771–1782, Jul. 2003.
- [46] I. Yamada. The hybrid steepest descent method for the variational inequality problem over the intersection of fixed point sets of nonexpansive mappings. In *Inherently Parallel Algorithms for Feasibility and Optimization and their Applications*, pages 473–504. Elsevier, 2001.
- [47] K. Slavakis, I. Yamada, and N. Ogura. The adaptive projected subgradient method over the fixed point set of strongly attracting nonexpansive mappings. *Numerical Functional Analysis and Optimization*, 27(7-8):905–930, Nov. 2006.
- [48] P. Bouboulis, K. Slavakis, and S. Theodoridis. Adaptive learning in complex reproducing kernel Hilbert spaces employing Wirtinger’s subgradients. *IEEE Trans Neural Networks*, 23(3):425–438, Mar. 2012.
- [49] J. J. Moreau. Proximité et dualité dans un espace hilbertien. *Bull. Soc. Math. France*, 93:273–299, 1965.
- [50] I. Daubechies, M. Defrise, and C. De Mol. An iterative thresholding algorithm for linear inverse problems with a sparsity constraint. *Comm. Pure Applied Math.*, 57(11):1413–1457, Nov. 2004.
- [51] M. Figueiredo, R. Nowak, and S. Wright. Gradient projection for sparse reconstruction: application to compressed sensing and other inverse problems. *IEEE J. Selected Topics Signal Process.: Special Issue on Convex Optimization Methods for Signal Processing*, 5981(4):586–598, Dec. 2007.
- [52] A. Beck and M. Teboulle. A fast iterative shrinkage-thresholding algorithm for linear inverse problems. *SIAM J. Imaging Sci.*, 2(1):183–202, 2009.
- [53] M. Fornasier and C.-B. Schönlieb. Subspace correction methods for total variation and ℓ_1 -minimization. *IMA J. Numer. Anal.*, 47(8):3397–3428, 2009.
- [54] G. Steidl and T. Teuber. Removing multiplicative noise by Douglas-Rachford splitting methods. *J. Math. Imag. Vis.*, 36(3):168–184, 2010.
- [55] J.-C. Pesquet and N. Pustelnik. A parallel inertial proximal optimization method. *Pac. J. Optim.*, 8(2):273–305, Apr. 2012.
- [56] G. Chen and M. Teboulle. A proximal-based decomposition method for convex minimization problems. *Math. Program.*, 64:81–101, 1994.

- [57] E. Esser, X. Zhang, and T. Chan. A general framework for a class of first order primal-dual algorithms for convex optimization in imaging science. *SIAM J. Imaging Sci.*, 3(4):1015–1046, 2010.
- [58] A. Chambolle and T. Pock. A first-order primal-dual algorithm for convex problems with applications to imaging. *J. Math. Imag. Vis.*, 40(1):120–145, 2011.
- [59] L. M. Briceño-Arias and P. L. Combettes. A monotone + skew splitting model for composite monotone inclusions in duality. *SIAM J. Opt.*, 21(4):1230–1250, 2011.
- [60] P. L. Combettes and J.-C. Pesquet. Primal-dual splitting algorithm for solving inclusions with mixtures of composite, Lipschitzian, and parallel-sum type monotone operators. *Set-Valued Var. Anal.*, 2011.
- [61] B. C. Vũ. A splitting algorithm for dual monotone inclusions involving cocoercive operators. *Adv. Comput. Math.*, 38(3):667–681, April 2013.
- [62] L. Condat. A primal-dual splitting method for convex optimization involving Lipschitzian, proximable and linear composite terms. *J. Optim. Theory Appl.*, 158(2):460–479, August 2012.
- [63] P. Chen, J. Huang, and X. Zhang. A primal-dual fixed point algorithm for convex separable minimization with applications to image restoration. *Inverse Problems*, 29(2), 2013.
- [64] N. Pustelnik, J.-C. Pesquet, and C. Chaux. Relaxing tight frame condition in parallel proximal methods for signal restoration. *IEEE Trans. Signal Process.*, 60(2):968–973, Feb. 2012.
- [65] C. Couprie, L. Grady, L. Najman, J.-C. Pesquet, and H. Talbot. Dual constrained TV-based regularization on graphs. *SIAM Journal on Imaging Sciences*, 6(3):1246–1273, 2013.
- [66] S. Setzer, G. Steidl, and T. Teuber. Deblurring Poissonian images by split Bregman techniques. *J. Visual Communication and Image Representation*, 21(3):193–199, Apr. 2010.
- [67] M. A. T. Figueiredo and J. M. Bioucas-Dias. Restoration of Poissonian images using alternating direction optimization. *IEEE Trans. Image Process.*, 19(12):3133–3145, Dec. 2010.
- [68] M. V. Afonso, J. M. Bioucas-Dias, and M. A. T. Figueiredo. An augmented Lagrangian approach to the constrained optimization formulation of imaging inverse problems. *IEEE Trans. Image Process.*, 20(3):681–695, Mar. 2011.
- [69] S. Boyd, N. Parikh, E. Chu, B. Peleato, and J. Eckstein. Distributed optimization and statistical learning via the alternating direction method of multipliers. *Found. Trends Machine Learn.*, 8(1):1–122, 2011.
- [70] G. Peyré and J. Fadili. Group sparsity with overlapping partition functions. In *Proc. Eur. Sig. and Image Proc. Conference*, pages x+5, Barcelona, Spain, Aug. 29 – Sept. 2, 2011.
- [71] I. Ekeland and R. Témam. *Convex analysis and variational problems*. SIAM, Philadelphia, 1999.
- [72] P. L. Combettes and J.-C. Pesquet. Proximal thresholding algorithm for minimization over orthonormal bases. *SIAM J. Opt.*, 18(4):1351–1376, Nov. 2007.

- [73] F. Alizadeh and D. Goldfarb. Second-order cone programming. *Mathematical Programming*, 95:3–51, 2003.
- [74] U. Faraut and A. Korányi. *Analysis on Symmetric Cones*. Oxford Mathematical Monographs. Oxford University Press, New York, 1994.
- [75] J. S. Pang, D. F. Sun, and J. Sun. Semismooth homeomorphisms and strong stability of semidefinite and Lorentz complementarity problems. *Math. Oper. Res.*, 28:39–63, 2003.
- [76] J. Wu, F. Liu, L. C. Jiao, X. Wang, and B. Hou. Multivariate compressive sensing for image reconstruction in the wavelet domain. *IEEE Trans. Image Process.*, 20(12):3483–3494, Dec. 2011.
- [77] J.-F. Aujol. Some first-order algorithms for total variation based image restoration. *J. Math. Imag. Vis.*, 34(3):307–327, Jul. 2009.
- [78] B. A. Turlach, W. N. Venables, and S. J. Wright. Simultaneous variable selection. *Technometrics*, 47(3):349–363, Aug. 2005.
- [79] Y. Chen and A. O. Hero. Recursive $\ell_{1,\infty}$ lasso. *IEEE Trans. Signal Process.*, 60(8):3978–3987, Aug. 2012.
- [80] E. J. Candès, M. B. Wakin, and S. Boyd. Enhancing sparsity by reweighted ℓ_1 minimization. *J. Fourier Anal. Appl.*, 14(5):877–905, Dec. 2008.
- [81] I. Bayram and M. Kamasak. Directional total variation. *IEEE Signal Processing Letters*, 2012.
- [82] J. Eckstein. Parallel alternating direction multiplier decomposition of convex programs. *J. Optim. Theory Appl.*, 80(1):39–62, 1994.
- [83] M. V. Afonso, J. M. Bioucas-Dias, and M. A. T. Figueiredo. Fast image recovery using variable splitting and constrained optimization. *IEEE Trans. Image Process.*, 19(9):2345–2356, 2010.
- [84] P. Weiss, L. Blanc-Féraud, and G. Aubert. Efficient schemes for total variation minimization under constraints in image processing. *SIAM J. Sci. Comput.*, 31(3):2047–2080, April 2009.
- [85] J. M. Fadili and G. Peyré. Total variation projection with first order schemes. *Trans. Img. Proc.*, 20(3):657–669, March 2011.
- [86] A. Buades, B. Coll, and J. Morel. A review of image denoising algorithms, with a new one. *Multiscale Model. and Simul.*, 4(2):490–530, 2005.
- [87] S. Mallat. *A wavelet tour of signal processing*. Academic Press, San Diego, USA, 1997.
- [88] J.-F. Cai, B. Dong, S. Osher, and Z. Shen. Image restoration: Total variation, wavelet frames and beyond. *J. Amer. Math. Soc.*, 25(4):1033–1089, 2012.
- [89] X. Zhang, M. Burger, X. Bresson, and S. Osher. Bregmanized nonlocal regularization for deconvolution and sparse reconstruction. *SIAM J. Imaging Sci.*, 3(3):253–276, 2010.
- [90] G. Peyré, S. Bogleux, and L. D. Cohen. Non-local regularization of inverse problems. *Inverse Problems and Imaging*, 5(2):511–530, 2011.

- [91] G. Peyré. A review of adaptive image representations. *IEEE Journal of Selected Topics in Signal Processing*, 5(5):896–911, Sep. 2011.
- [92] A. Foi and G. Boracchi. Foveated self-similarity in nonlocal image filtering. In *Proc. SPIE Electronic Imaging 2012, Human Vision and Electronic Imaging XVII*, volume 8291, Burlingame (CA), USA, Jan. 2012.
- [93] G. Gilboa and S. Osher. Nonlocal linear image regularization and supervised segmentation. *Multiscale Model. and Simul.*, 6(2):595–630, 2007.
- [94] Z. Wang and A. C. Bovik. Mean squared error: love it or leave it? *IEEE Signal Process. Mag.*, 26(1):98–117, Jan. 2009.
- [95] R. A. Nobakht and M. R. Civanlar. Optimal pulse shape design for digital communication systems by projections onto convex sets. *IEEE Trans. Commun.*, 43(12):2874–2877, Dec. 1995.
- [96] P. L. Combettes and P. Bondon. Hard-constrained inconsistent signal feasibility problems. *IEEE Trans. Signal Process.*, 47(9):2460–2468, Sep. 1999.
- [97] R. Tibshirani. Regression shrinkage and selection via the lasso. *J. R. Statist. Soc. B*, 58:267–288, 1996.
- [98] M. Yuan and Y. Lin. Model selection and estimation in regression with grouped variables. *J. R. Statist. Soc. B*, 68:49–67, 2006.
- [99] R. Gaetano, G. Chierchia, and B. Pesquet-Popescu. Parallel implementations of a disparity estimation algorithm based on a proximal splitting method. In *Visual Communication and Image Processing*, San Diego, USA, 2012.